Student Poster Presentation on Hydrogen and Fuel Cells

within the 13th International Summer School on Advanced Studies of Polymer Electrolyte Fuel Cells

Graz University of Technology, September 7th, 2021

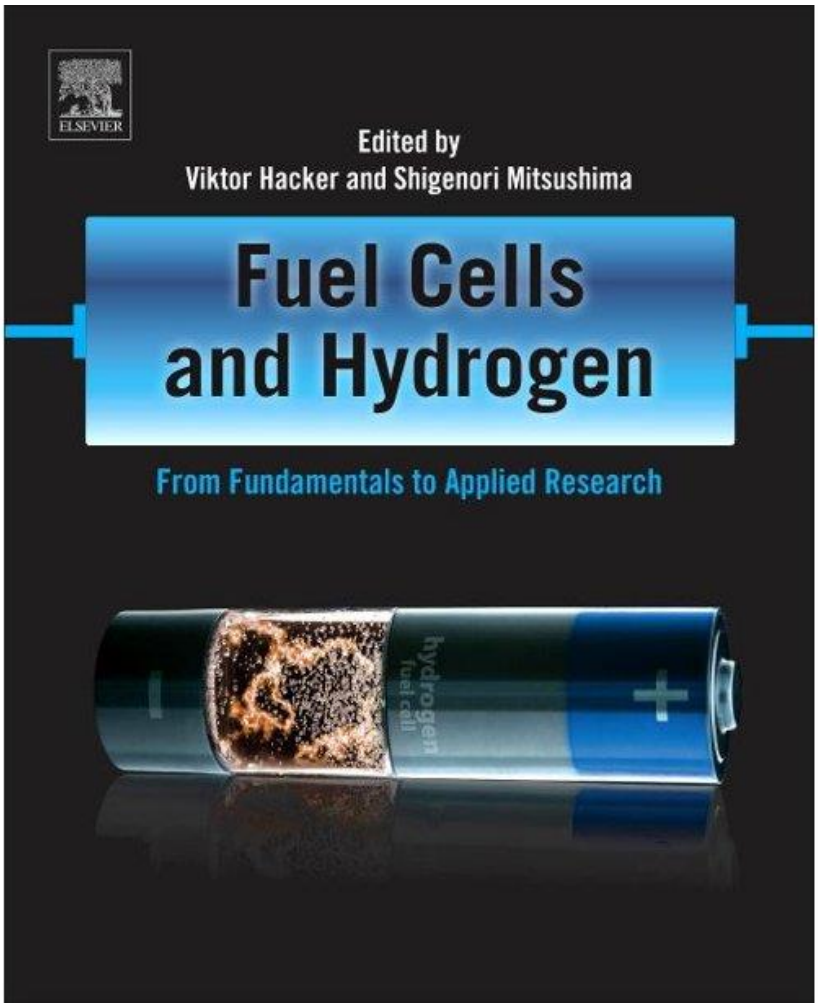

Fuel Cells and Hydrogen: From Fundamentals to Applied Research
Viktor HACKER, Shigenori MITSUSHIMA (eds.)
ISBN: 9780128114599, Elsevier 296 pages, 19th July 2018.

Fuel Cells and Hydrogen: From Fundamentals to Applied Research provides an overview of the basic principles of fuel cell and hydrogen technology, which subsequently allows the reader to delve more deeply into applied research. In addition to covering the **basic principles of fuel cells** and hydrogen technologies, the book examines the principles and methods to **develop and test fuel cells**, the evaluation of the **performance** and **lifetime** of fuel cells and the concepts of **hydrogen production**. *Fuel Cells and Hydrogen: From Fundamentals to Applied Research* acts as an invaluable reference book for **fuel cell developers** and **students**, researchers in **industry** entering the area of fuel cells and lecturers teaching fuel cells and hydrogen technology.

Contents

Poster Abstracts

STUDY ON THE PRODUCTION PARAMETERS OF MEMBRANE ELECTRODE ASSEMBLIES AND THE INFLUENCE ON THE PERFORMANCE IN ALKALINE DIRECT ETHANOL FUEL CELLS

BILLIANI Andreas, ROSCHGER Michaela, WOLF Sigrid and HACKER Viktor

Institute of Chemical Engineering and Environmental Technology, Graz University of Technology, Austria, andreas.billiani@tugraz.at

Keywords: alkaline direct ethanol fuel cells, ethanol, renewable resources, polarization curve.

INTRODUCTION

Since the industrial revolution, a rapid increase in population and energy demand has taken place. This led to the need for alternative ways of energy production. Fuel cells are a versatile method for the sustainable production of electrical energy, using fuels synthesized from a renewable feedstock, such as second-generation bioethanol [1].

Alkaline direct ethanol fuel cells (ADEFC) offer a promising alternative to their well-established hydrogen-based counterparts, as the production of ethanol is less energy intensive and as a liquid fuel, the logistical infrastructure is already pre-existing. Furthermore, the use of KOH as an alkaline electrolyte allows the employment of cheaper non-noble metal catalysts [2]. Nevertheless, there are also drawbacks linked to ethanol as a fuel. Firstly, the catalysts that are currently in use are not able to complete the oxidation of EtOH to CO_2 and H_2O yielding $12e^-$ (Eq. 1). Instead, the incomplete conversion to acetate as a side product takes place, releasing only $4e^-$, reducing the efficiency through kinetic limitations (Eq. 2).

$$CH_3CH_2OH + 12\ OH^- \rightarrow 2CO_2 + 9H_2O + 12e^- \quad (1)$$

$$CH_3CH_2OH + 5\ OH^- \rightarrow CH_3COO^- + 4H_2O + 4e^- \quad (2)$$

Secondly, another major problem is the crossover of ethanol through the membrane from the anode to the cathode driven by the osmotic drag. This phenomenon causes the formation of mixed potentials which results in a decrease of the power density [3].

The aim of this study is to combine the currently existing approaches in literature to increase the performance of the fuel cells such as: operating temperature, catalyst type and loading, as well as the nature of the membrane in use and the fabrication of the membrane electrode assembly (MEA) itself (Fig. 1).

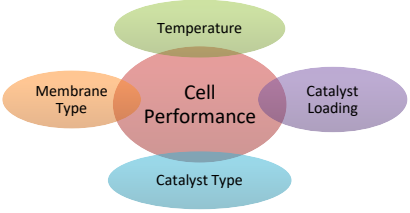

Fig. 1: Criteria that influence the cell performance

EXPERIMENTAL

The anode catalysts were synthesized via the modified instant reduction method [4]. An ink was fabricated by dispersing the catalyst powder in isopropanol, ultrapure water and an ionomer, acting as the binder. Subsequently, the ink was applied evenly on the backing layers (carbon cloth for the anode and carbon paper for the cathode) using a SONO-TEK® ultrasonic spray coater (Fig. 2). The electrodes were combined with the membrane without any mechanical procedure, just by the cohesion of the cell itself to produce the MEA. Different commercial membranes from fumasep® (FAA-3-50 and FAA-3-PK130) were used and their influence on the performance at two operational temperatures (RT, 80°C) was tested. The measurements were conducted with a Thales TX potentiostat from Zahner-elektrik GmbH&Co KG®.

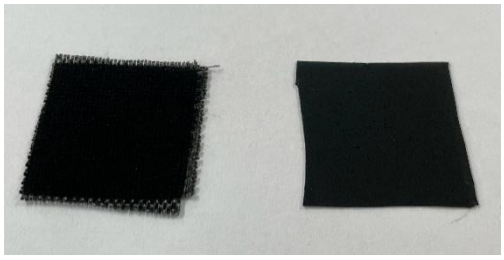

Fig. 2: Anode (left) and cathode (right) after the spray coating process

RESULTS

At RT the power density for the measurement with the FAA-3-50 membrane was approx. 4-fold higher compared to the FAA-3-PK-130 membrane. When the temperature is raised to 80°C the situation is reversed as the FAA-3-PK-130 membrane delivers nearly twice the power output compared to the FAA-3-50. This phenomenon can be explained by the greater thickness (FAA-3-50: 50 µm and FAA-3-PK-130: 130 µm) and stability of the membrane as the PK-130 is reinforced.

ACKNOWLEDGEMENT

The authors acknowledge the financial support by the Austrian Science Fund (FWF): I 3871-N37.

REFERENCES

[1] S. Chu and A. Majumdar, Nature, 2012, 294-303.
[2] T. S. Zhao, Y. S. Li and S. Y. Shen, Front. Energy Power Eng. China, 2010, 443-458.
[3] B.Cermenek, J.Ranninger, V.Hacker; In Ethanol: Science and Engineering, A.Basile, A.Iulianelli, F.Dalena, N.T.Veziroglu, Eds.; Elsevier Inc.: Amsterdam, 2019, 383-405.
[4] B. Cermenek, B. Genorio, T. Winter, S. Wolf, J.G. Connell, M. Roschger, I. Letofsky-Papst, N. Kienzl, B. Bitschnau, V. Hacker, Electrocatalysis, 2020, 11, 203–214.

EVALUATION OF THE DEGRADATION OF CATALYST COATED NI ANODES FOR OXYGEN EVOLUTION IN ALKALINE WATER ELECTROLYSIS USING ADT BASED ON REVERSE CURRENT PHENOMENON

ENJOJI Hayato[1], HALEEM Ashraf Abdel[2], NAGASAWA Kensaku[2], KURODA Yoshiyuki[1,2] and MITSUSHIMA Shigenori [1,2]

[1]Graduate School of Engineering Science, Yokohama National University, 79-5 Tokiwadai, Hodogaya-ku, Yokohama 240-8501, Japan
[2]Institute of Advanced Sciences, Yokohama National University, 79-5 Tokiwadai, Hodogaya-ku, Yokohama 240-8501, Japan, cel@ml.ynu.ac.jp

Keywords:. Alkaline Water Electrolysis, Reverse Current, Ni based Electrode, accelerated durability test

INTRODUCTION

Power to Gas (P2G) technology is expected to allow installation of a lot of renewable electricity without imbalance issue of electric power grid. Here, water electrolysis is a key device in the P2G. One of the conventional methods in water electrolysis is alkaline water electrolysis (AWE), which has the advantages of a low-cost material electrolyzer. On the other hand, there is an issue of electrode degradation caused by the reverse current generated by frequent start-stop of renewable energy power source. Therefore, further understanding of degradation phenomenon and development of durable electrodes are needed.

In this study, degradation of NiCo spinel catalyst coated Ni anode (electrode A) and Ni-Co-Ir oxide catalyst with LiNi oxide interlayer coated Ni anode (electrode B) have been investigated using Accelerated Durability Test (ADT) based on reverse current phenomenon [1]. The effect of stop condition of Emin and short open circuit potential (OCP) holding before reverse current mode on degradation have been discussed with cyclic voltammetry (CV) as electrochemical measurement.

EXPERIMENT

ADT was performed in a three-electrode cell with 7 M KOH aqueous as electrolyte at 25 oC. RHE, Ni coil and 1 cm^2 electrode A, B are used as reference, counter and working electrodes, respectively. Constant current electrolysis at 1 A cm^{-2} for 2 hours was conducted as pretreatment at 80 °C before ADT. The ADT protocol consisted of three steps: (1) constant current electrolysis at 600 mA cm^{-2} for 1 min, (2-1)0 or 10 s at open-circuit potential (OCP) for without and with OCP, (2-2) potential scanning from OCP to anodic potential E_{min} (=0.5 V vs. RHE) at scanning rate of -0.5 V s^{-1}, and (3) holding at constant potential of E_{min} for 1 min as shown in Fig. 1.

To evaluate the oxygen evolution activity, CV (potential range: 0.5-2.0 V, scanning speed: 5, 50 mV s^{-1}, 3 cycles) and AC impedance measurements (bias potential: 1.6, 1.7 V, frequency range: 10^{6}-10^{-1} Hz, amplitude: 10 mV) were performed basically at

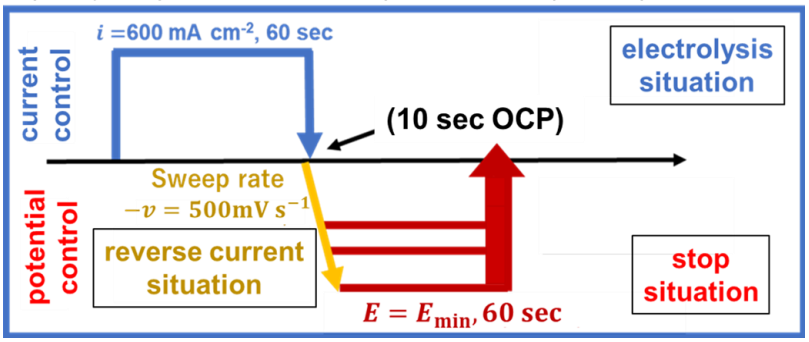

Fig. 1 ADT protocol outline drawing.

every 200 ADT cycles in 2,000 cycles of ADT. Furthermore, the same degradation evaluation was performed by the protocol inserting 10 s holding at OCP between (1) and (2) at E_{min} = 0.5 V vs. RHE to evaluate relaxation effect.

RESULTS & DISCUSSIONS

Fig. 2 shows the *iR*-free anode potential of CV at i =100 mA cm^{-2} as a function of the ADT cycles with and without 10 s of OCP at E_{min} = 0.5 V. About electrode A, the anode potential increased from ca. 1.6 to 1.8 V vs. RHE during 2,000 cycles of the ADT. The potential increase of electrode B is less than that of electrode A. Anode potentials with and without OCP after ADT were almost same. However, potential with OCP was significantly smaller than that without OCP in the early cycle of the ADT about electrode A.

Fig. 3 shows the anodic peak potential of the CV as a function of the ADT cycles about electrode A. As inset of Fig. 3, the CV had two anodic peaks of (1) α-$Ni(OH)_2$/γ-NiOOH at E_0 =1.33 V vs. RHE, and (2) β-$Ni(OH)_2$/β-NiOOH at E_0 =1.39 V vs. RHE. The peaks (1) corresponds to more active site, and peak (2) corresponds to less active site than peak (1) [2]. Therefore, the increase of the (2) and the decrease of the (1) with the ADT cycles would correspond to the degradation. In the early cycles, the peak currents with OCP were more active side than that without OCP.

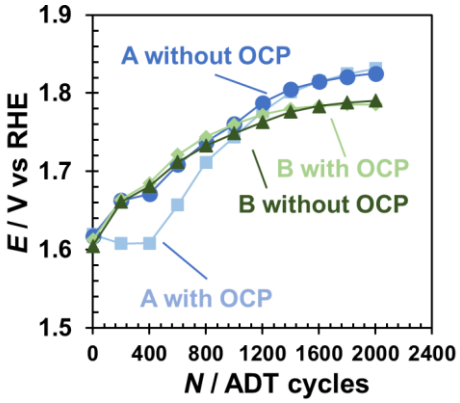

Fig. 2 ADT cycle dependence of anode potential by protocol with and without OCP.

Fig. 4 shows the Ir_2O_3/IrO_2 oxidation peak current from CV at E = 0.57 V vs. RHE and for electrode B and β-$Ni(OH)_2$/β-NiOOH oxidation peak current at E = 1.39 V vs. RHE for the electrode A and B as a function of ADT cycle without OCP. The anode potential of the electrode B increased in early ADT cycles as shown Fig. 1. Simultaneously, the peak current of

Ir decreased. This would indicate that Ir amount rapidly decrease by about 200 cycles, so the activity decrease in early period would strongly correspond to the Ir amount. However, final potential of electrode B was lower than that of A. As shown

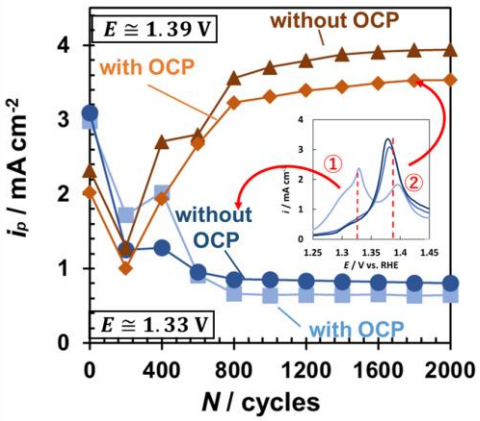

Fig. 3 ADT cycle dependence of Ni anodic peak current.

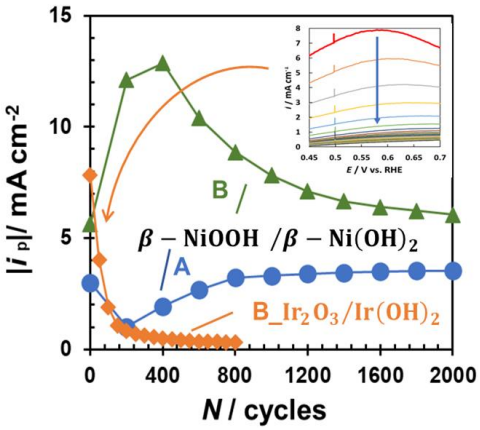

Fig. 4 ADT cycle dependence of peak currents at $\boldsymbol{E}$=**0.57 V** (Ir_2O_3/IrO_2) and $\boldsymbol{E}$=**1.39V** (β-NiOOH /β-$Ni(OH)_2$).

by the β-$Ni(OH)_2$/β-NiOOH peak currents in Fig. 4, larger amount of β-$Ni(OH)_2$/β-NiOOH site on the electrode B, which would work as active site, remained after ADT. Therefore, the intermediate layer of electrode B would contribute to suppress potential increase.

Conclusively, it is suggested that the degradation is a combination of multiple processes, and it is possible that the components are selectively reduced. The insertion of OCP to suppress the potential increase would be affected by not only coherency of catalyst layer to suppress detachment but also the activation of catalyst itself.

ACKNOWLEDGEMENTS

This study was based on results obtained from the Development of Fundamental Technology for Advancement of Water Electrolysis Hydrogen Production in Advancement of Hydrogen Technologies and Utilization Project (JPNP14021) commissioned by the New Energy and Industrial Technology Development Organization (NEDO).

REFERENCES

[1] A. Abdel Haleem, K. Nagasawa, Y. Kuroda, Y. Nishiki, A. Zaenal, and S. Mitsushima, Electrochemistry, 89, 186 (2021).

[2] K. Juodkazis, J. Juodkazyte, R. Vilkauskaite, V. Jasulaitiene, J. Solid State Electrochem., 12, 1469 (2008).

EVALUATION METHOD OF GAS PERMEABILITY OF MEMBRANES FOR ALKALINE WATER ELECTROLYSIS

FURUTA Rina[1], NAGASAWA Kensaku[2], KURODA Yoshiyuki[1,2] and MITSUSHIMA Shigenori[1,2]

[1]Graduate School of Engineering Science, Yokohama National University, 79-5 Tokiwadai, Hodogaya-ku, Yokohama 240-8501, Japan, cel@ml.ynu.ac.jp
[2]Institute of Advanced Sciences, Yokohama National University, 79-5 Tokiwadai, Hodogaya-ku, Yokohama 240-8501, Japan, cel@ml.ynu.ac.jp

Keywords: Alkaline water electrolysis; Separator membrane; Gas permeability; Diffusion

INTRODUCTION

Alkaline water electrolysis (AWE) has attracted much attention as a low cost and large-scale production process of H_2 from renewable energy. In order to realize the hydrogen society, further reduction of costs and improvement of efficiency are required. H_2 and O_2 evolved by AWE are separated by electrolyte absorbed porous membrane such as Zirfon® PERL, the commercially available membrane composed of polysulfone and zirconia. High ionic conductivity and low gas permeability are required for the membranes. Thus, the evaluation of the gas permeability of membrane is regarded as an important issue. [1]

In this study, we designed a new electrochemical cell (membrane evaluation cell), consisting of water electrolysis system and H_2 detection system, for the evaluation of gas permeability of membranes.

EXPERIMENTAL

Fig. 1 shows the schematic structure of the membrane evaluation cell. This cell consists of water electrolysis system to generate electrolytic H_2 bubbles and H_2 detection system to measure H_2 diffusing through the membrane. Nafion® 117 (DuPont) was used as a separator in each system. Zirfon® PERL UPT 500 (Agfa) was set between the cathode chamber of the water electrolysis system and the anode of the H_2 detection system.

H_2 bubbles were supplied to the cathode chamber of the water electrolysis system by water electrolysis (30 mA cm^{-2}) or 6 - 7 cm^3min^{-1} of bubbling. At the same time, constant voltage (0.10 - 0.85 V) was applied to the H_2 detection system to detect oxidation current of dissolved H_2 diffusing throughout the membrane. Hereafter, cathode chamber of the water electrolysis system is denoted as the H_2 supply chamber, and the anode and cathode of the H_2 detection system are denoted as H_2 detection, and counter

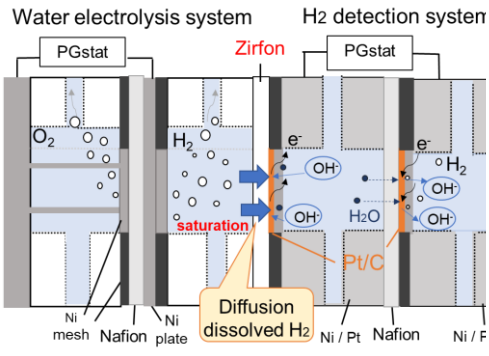

Fig. 1 Schematic illustration of the membrane evaluation cell.

electrodes, respectively. A 1.0 - 5.0 M (= mol dm^{-3}) KOH solution was fed as the electrolyte to each electrode chamber at ambient temperature and pressure.

Electrochemical H_2 determination was performed as follows. For a background measurement, current density of the H_2 detection system (i_{bkg}) was recorded until steady state at each cell voltage without the supply of H_2 in the water electrolysis system. For a permeability measurement, H_2 is generated or bubbled in the H2 supply chamber and the current density of the H_2 detection system (i) was recorded until steady state at each cell voltage. The H_2 oxidation current density ($i_{\mathrm{H_2}}$) was obtained by subtracting i_{bkg} from i.

RESULTS AND DISCUSSION

Fig. 2 shows i_{bkg} and $i_{\mathrm{H_2}}$ when H_2 was generated by water electrolysis. In high cell voltage, $i_{\mathrm{H_2}}[1]$ showed diffusion limited current but some of its values and $i_{\mathrm{H_2}}[2]$ had errors. To solve the problem, H_2 supply chamber was investigated, because the concentration of OH^- in the H_2 supply chamber gradually was increased by electro-osmic drag water of Nafion during electrolysis. Then, both H_2 solubility and diffusion coefficient of H_2 in KOH solution decrease, the amount of dissolved hydrogen permeating through Zirfon also decrease. Therefore, H_2 was supplied by bubbling, in which H_2 is supplied without increasing the concentration of OH^-. However, the bubbling did not decrease the error in $i_{\mathrm{H_2}}$ enough.

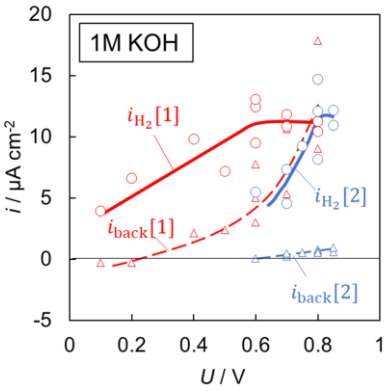

Fig. 2 Background (i_{back}) and H_2 oxidation ($i_{\mathrm{H_2}}$) current densities as a function of cell voltage of the H_2 detection system.

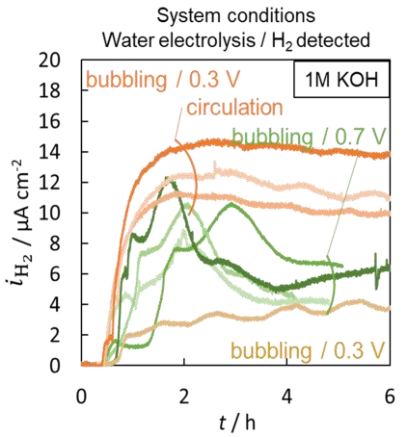

Fig. 3 Time course behaviors of the H_2 oxidation current density ($i_{\mathrm{H_2}}$) with and without circulation of electrolyte.

We focused on the errors in the H_2 detection system. Cell voltage U is expressed as

$$U = \Delta E + i(R_{mass\ trans} + R_{ct-a} + R_{ct-b} + R_{membrane}) \quad (1)$$

where ΔE, $R_{mass\ trans}$, R_{ct-a}, R_{ct-b}, and $R_{membrane}$ denote the difference in the equilibrium potentials between H2 detection electrode and counter electrode, mass transfer resistance of H_2 in the Zirfon, charge transfer resistances of H_2 detection and counter electrodes, and the membrane resistance, respectively. The overall resistance was dominated by $R_{mass\ trans}$. If evolved H_2 accumulated on the counter electrode, ΔE

has a positive value. Because a constant cell voltage: U is applied on the H_2 detection system, the current density: i decreases due to potential decrease of the counter electrode by the H_2 concentration increase. Therefore, the electrolyte supplied to the cathode chamber of the H_2 detection system was circulated to remove trapped H_2 on the counter electrode. The i_{H_2} recorded with the circulation of the electrolyte was more stable than those recorded without the circulation (Fig. 3), which implies that the unstability of the counter electrode potential affected i_{H_2}. Thus, we plan to control the potential of the H_2 detection electrode, using a reference electrode.

REFERENCES

[1] M. Schalenbach, W. Lueke, D. Stolten, J. Electrochem. Soc., 163, 14 (2016).

BIOPOLYMER BASED ANION EXCHANGE MEMBRANES FOR THE USE IN ALKALINE ANION EXCHANGE MEMBRANE FUEL CELLS

HREN Maša[1] and GORGIEVA Selestina[2]

[1]Faculty of Mechanical Engineering, University of Maribor, Smetanova 17, 2000 Maribor, Slovenia, masa.hren@um.si
[2]Faculty of Electrical Engineering and Computer Science, University of Maribor, Koroška cesta 46, 2000 Maribor, Slovenia, selestina.gorgieva@um.si

Keywords: Functionalized nanofibrillated cellulose, alkaline fuel cell, anion exchange membrane, biopolymer membrane

Alkaline anion exchange membrane fuel cells (AAEMFC) are attracting ever-increasing attention, as they are promising electrochemical devices for energy production, presenting a viable opponent to the more researched proton exchange membrane fuel cells. [1] In principle, AAEMFCs allow for the use of non-precious metal catalysts, which dramatically reduces the cost per kilowatt of power in fuel cell devices. The heart of a AAEMFC is the membrane electrode assembly consisting of an anion exchange membrane (AEM) sandwiched between an anode and a cathode. Currently, the commercially available AEMs do not possess satisfactory properties which would allow for the commercial breakthrough of alkaline fuel cells. This indicates a need for the development of new highly efficient, environmentally friendly and economically viable AEMs. Synthesis of synthetic polymer AEMs is usually complex and time consuming, as well as environmentally unfriendly. Therefore, it is highly desired that the membrane material is renewable and environmentally benign. Naturally derived materials are an alternative, where chitosan (CS), nanofibrillated cellulose (CNF) and nanocrystalline cellulose have been, up to now, proposed as promising. [2,3] They can be modified readily by the attachment of different moieties. Currently, despite all the presented benefits, biopolymer AEMs are still not advantageous in comparison to synthetic AEMs, especially in terms of ionic conductivity and mechanical properties, which can be improved by the introduction of fillers.

The goal of this research was to prepare and characterize a series of biopolymer membranes as AEMS for the use in AAEMFCs. The AEMs were designed by a simple, cost-effective, solution-casting procedure, fully complying with green-chemistry principles. In this work, CNF was functionalized with a quaternary ammonium group bearing agent poly(diallyldimethylammonium chloride) (polyDADMAC) with the intent of introducing a permanently positively charged quaternary ammonium moiety onto CNF. The functionalized polyDADMAC CNF and pure CNF were used as fillers in chitosan membranes. The chitosan membrane mixtures were prepared with varying contents of CNF and the polyDADMAC modified CNF and casted as membranes. The so obtained membranes were characterized by ion exchange capacity determination, ethanol permeability, mechanical testing as well as its swelling ratio and alkaline uptake properties.

REFERENCES

[1] M. Hren, M. Božič, D. Fakin, K. S. Kleinschek, and S. Gorgieva, “Alkaline membrane fuel cells: Anion exchange membranes and fuels,” Sustain. Energy Fuels, vol. 5, no. 3, pp. 604–637, 2021.

[2] S. Gorgieva et al., “Efficient chitosan/nitrogen-doped reduced graphene oxide composite membranes for direct alkaline ethanol fuel cells,” Int. J. Mol. Sci., vol. 22, no. 4, pp. 1–25, 2021.

[3] M. Hren et al., “Chitosan-Mg(OH)2 based composite membrane containing nitrogen doped GO for direct ethanol fuel cell,” Cellulose, vol. 28, no. 3, pp. 1599–1616, 2021.

MEMS SENSOR DEVELOPMENT FOR MAKING PEFC CATALYST LAYER DURING DRYING PROCESS

HYUGAJI Yoshifumi[1], ASAOKA Kota[1] and ARAKI Takuto[2]

[1]Graduate School of Eng., Yokohama National University, Japan, hyugaji-yoshifumi-st@ynu.jp, asaoka-kota-xs@ynu.jp
[2]Faculty of Eng., Yokohama National University, Japan, taraki@ynu.ac.jp

Keywords: PEFC, Catalyst, Micro sensor, Impedance

INTRODUCTION

PEFC(Polymer Electrolyte Fuel Cell) has attracted attention as energy devise which does not discharge CO2. The CL(Catalyst Layer) of PEFC has complicated making process due to many physical phenomena such like condensation of particles, generation of microporous and drying of solvent [1], therefore now the way of CL development is that engineer make and test a lot of conditions one after another then get feedback and improve the development, which has problems of cost and dependence on developer's experience. In order to improve this situation, Nagato et al. have applied machine learning to CL making process [2]. With them, we developed impedance measurement sensor and automated measurement method for drying process in CL making.

EXPERIMENTAL METHOD

The schematic of micro sensor is shown in Fig. 1. The basis wafer is 425 µm thickness SiO_2 with 1µm thickness coating of thermal oxidation film. Sensor electrodes are consisted of chromium processed by RF(Rapid-Frequency) Magnetron Sputtering and photolithography and the insulator layer upon the electrodes was SiO_x also obtained by RF Magnetron Sputtering with SiO_2 target. We used Shenzhen Yuejiang Technology DOBOT Magician for automation of experiment. When impedance measurement, the arm of DOBOT moved to connection points to connect pin tip to sensor terminal. The pin was also connected by lead line to HIOKI IM3590 LCR meter. DLAB dPette 5-50 was used for dropping the ink. To control the electric pipet, DC 5V output from DOBOT ex-I/O pin was used. PC with python program was connected to 2 DOBOTs and LCR meter by USB cable. OMRON E5CC thermal controller was connected to DC 3.3V output and GND on DOBOT ex-I/O pin and temperature set point was controlled by output voltage.

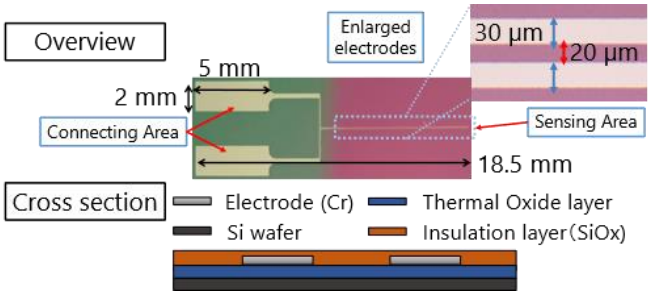

Fig. 1 Schematic figure of micro sensor

The base ink was consisted of Vulcan XC-72RR 5g, Chemours Nafion 5wt% solution 49 mL, deionized water 11.8mL, 2-propanol 15mL and the imitation catalyst ink used in experiment was obtained by diluting base ink adding 2-propanol 3 times as heavy as base ink. The prepared imitation ink was stirred and degassed by THINKY ARE-310 through 5 minutes 800 r.p.m. rotation and 2000 r.p.m. revolution and 5minutes 2000 r.p.m. revolution then dispersed 10 minutes by Branson SFX250 with 10% amplitude. Each experiment were conducted with 30μL of the ink.

RESULTS AND DISCUSSION

The temperature conditions were that preheat at 30℃ during 30s from dropping then temperature set points were changed every 60 seconds till 510s, for 2 patterns, „2step heat“ was set to 30, 70, 80, 30, 90℃, „High heat“ was set to 90, 50, 50, 60, 70℃. The impedance measurement data was processed to nondimensionalization. On each temperature conditions, the average and standard deviation of 5 measurement data of impedance and phase angle are shown in Fig. 2, impedance of “High heat” decrease from start to 140s and “2 step heat” to 180s. These trends can be explained by volumetric contraction of ink droplet. The solvent in ink evaporates with being heated, at the same time, conductive ingredients such as carbon and ionomer move to near the electrodes with contraction of ink droplet. This phenomenon leads to increasement of capacity because the electric field density is higher near the electrodes, so impedance decreases with increasement of capacity. This estimation is also supported by considering about quantity of heat, “High heat” is given larger quantity of heat due to higher temperature set value from 30s to 150s thus the impedance decrease time was shorter. After the minimum point of impedance value, impedance increased with progress of drying, the maximum point was 400s for “2 step heat”, 260s for “High heat”. These increasement were considered to have been effects of dispersion of conductive ingredients in ink from electrode vicinity due to farther heating.

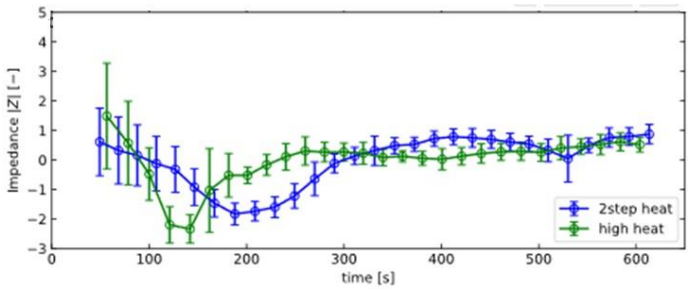

Fig. 2 Dimensionless Impedance acquired at 1226 Hz while ink drying with heating

REFERENCES

[1] Kumano N et al, “Controlling cracking formation in fuel cell catalyst layers,” Journal of Power Sources, 419, pp. 219-228, (2019). Journal Paper

[2] Nagato K et al, Science of Machine, 72, pp. 511–516, (2020). Edited Book

RELATIONSHIP BETWEEN EVALUATION OF OER PERFORMANCE AND OXYGEN BUBBLE GENERATION BEHAVIOR IN ALKALINE WATER ELECTROLYSIS

IKEDA Hayata[1], MISUMI Ryuta[2] and MITSUSHIMA Shigenori[2,3]

[1]Graduate School of Engineering Science, Yokohama Natl. Univ., 79-5 Tokiwadai, Hodogaya-ku, Yokohama, 240-8501, Japan
[2]Faculty of Engineering, Yokohama Natl. Univ., 79-5 Tokiwadai, Hodogaya-ku, Yokohama, 240-8501, Japan
[3]Institute of Advanced Sciences, Yokohama Natl. Univ., 79-5 Tokiwadai, Hodogaya-ku, Yokohama, 240-8501, Japan

Keywords: Alkaline water electrolysis, Oxygen evolution reaction, Hydrogen production, Micro-bubble

INTRODUCTION

Alkaline Water Electrolysis (AWE) is anticipated as a mean of producing hydrogen as an energy carrier for sustainable development goals. One of the problems in alkaline water electrolysis is the rise in anode overvoltage at the high current density range. To further improve the efficiency of hydrogen production, grasping the bubble generation behavior and development of electrode materials based on it are important. In this study, using nickel electrodes with different diameters, the formation behavior of oxygen bubbles on the electrodes was observed with a high-speed video camera, and the relationship between the current density / electrode potential and the bubble formation behavior was investigated.

EXPERIMENTAL

Working electrode were Ni wire (NiW) (two types with diameters of 100 and 200 μm). A reference and a counter electrode were a reversible hydrogen electrode (RHE) and Ni rods (diameter 3 mm), respectively. All measurements were performed with a three-electrode electrochemical cell [1] at 303±1 K with KOH aqueous solution. To reduce the solution resistance as much as possible, the working electrode and the reference electrode were placed as close as possible (about 1 mm). To equalize the current density distribution, Ni rods counter electrode were inserted from both sides of the cell. Observation windows were fitted on the sides of the cell. The working electrode was exposed only the horizontal part about 3 mm where we want to observe the electrolytic reaction, and the other parts were covered by PTFE heat-shrink tube and epoxy resin. After appropriate pretreatments, cyclic voltammetry (CV) measurement was performed at a scan rate of 5 mV s^{-1} to obtain polarization curves. Electrochemical impedance spectroscopy (EIS) measurement was performed at 1.5-1.8 V vs. RHE with a potential amplitude 10 mV, a frequency range of 1×10^{0}-3×10^{5} Hz and 20 repeated measurements for each frequency. The solution resistance was obtained from the Nyquist plots, and the potential loss was corrected. The current density i_{geo} / A cm^{-2} was normalized by the geometric surface area of the cylindrical shaped working electrode. Constant current electrolysis was performed under five conditions of i_{geo} = 0.05-1.0 A cm^{-2}. Under each condition, the formation behavior of oxygen bubbles was

photographed with a high-speed video camera. From the obtained photographed images, the diameters of hundreds of oxygen bubbles detached from the electrodes were analyzed to calculate the Sauter mean diameter d_{32}.

RESULTS AND DISCUSSION

Fig. 1 shows the polarization curves of the Ni wire electrodes with different diameters. In the range of i_{geo} < 0.3 A cm^{-2} where the logarithmic value of the current density i_{geo} changed linearly with respect to the potential, there was no significant difference in an OER performance among the two types of electrodes. In the range of i_{geo} > 0.3 A cm^{-2}, the overvoltage increased with i_{geo} regardless of the electrode diameter, and it was confirmed that the smaller the diameter of the electrode was, the smaller the overvoltage at the same current density was, especially in the high current density range.

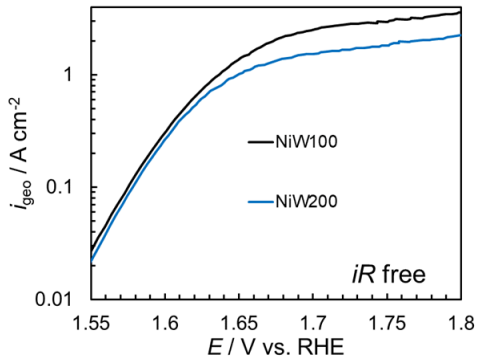

Fig. 1 Polarization curves with different electrode diameters from CV with scan rate 5 mV s^{-1}.

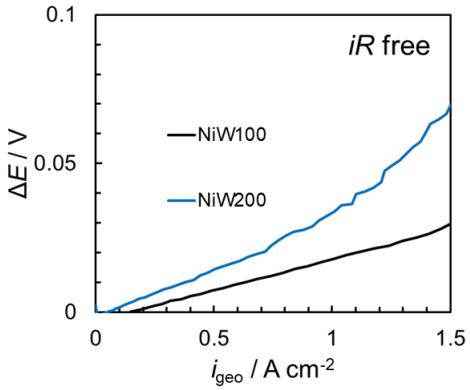

Fig. 2 Relationship between current density i_{geo} and overvoltage Δ*E* with different electrode diameters.

Fig. 2 shows the relationship between current density and overvoltage. It was confirmed that the overvoltage increased as the current density increased, and the smaller the surface curvature of the electrode was, the larger the overvoltage was. Fig. 3 shows the relationship between the current density and oxygen bubble diameter. The larger the current density was, the larger the oxygen bubble diameter was, and the oxygen bubble diameter was in proportion to the 1/3 power of i_{geo}. From the in-situ observation of the oxygen bubble generation behavior on the electrode with a high-speed video camera [2], the oxygen bubbles generated on the electrode coalesced and detached from the upper end of the Ni wire electrode placed horizontally. From the above, it was considered that the larger the surface curvature of the electrode was, i.e. the smaller the electrode diameter was, the smoother the detachment of oxygen bubbles from the electrode was. It is implied that large curvature of electrode surface contributed to the smaller overvoltage.

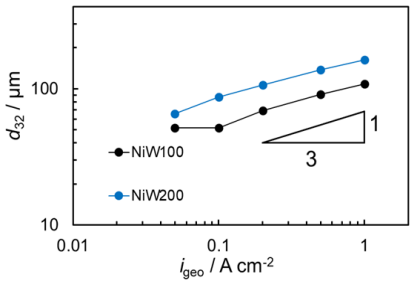

Fig. 3 Relationship between current density i_{geo} and oxygen bubble diameter d_{32} with different electrode diameters.

ACKNOWLEDGEMENTS

A part of this study was based on results obtained from the Development of Fundamental Technology for Advancement of Water Electrolysis Hydrogen Production in Advancement of Hydrogen Technologies and Utilization Project (JPNP14021) commissioned by the New Energy and Industrial Technology Development Organization (NEDO).

REFERENCE

[1] Y. Kojima, R. Misumi, M. Kaminoyama, S. Mitsushima, 43rd Electrolysis Technology Debate, 14 (2019)

[2] H. Ikeda, Y. Kojima, R. Misumi, M. Kaminoyama, S. Mitsushima, 22nd Society of Chemical Engineers Student Presentation, D08 (2020)

EVALUATION OF ANODE POROUS TRANSPORT LAYER USING POLARIZATION SEPARATION METHOD ON PEM WATER ELECTROLYSIS

ISHIDA Taiki[1], NAGASAWA Kensaku[2], KURODA Yoshiyuki[1,2] and MITSUSHIMA Shigenori[1,2]

[1]Graduate school of Engineering Science, Yokohama National University, 79-5 Tokiwadai, Hodogaya-ku, Yokohama 240-8501, Japan, email: cel@ml.ynu.ac.jp
[2]Institute of Advanced Sciences, Yokohama National University, 79-5 Tokiwadai, Hodogaya-ku, Yokohama 240-8501, Japan: cel@ml.ynu.ac.jp

Keywords: PEM water electrolysis, Porous transport layer, Polarization separation

INTRODUCTION

Recently, proton exchange membrane water electrolysis (PEMWE) has been expected as the hydrogen production technology to convert the renewable energy into hydrogen. PEMWE has high energy conversion efficiency even in high current density region, but improvements are still required to reduce cost due to the utilization of noble metals. The porous transport layer (PTL) is one of the most important elements to improve PEMWE. PTLs have the roles such as supplying water to catalyst layer (CL), discharging the generated gas, and transporting electrons between the CL and bipolar or end plates [1]. Therefore, the accurate separation and determination of the polarization in the electrolyzer are essential technologies. In that case, the potential measurement using reference electrodes can be useful. In this study, we measured the anode and cathode polarizations with correction of membrane resistance, and evaluated the polarization of two anode PTLs of platinized sintered Ti porous substrate with different pore size and porosity using a small size electrolyzer with double references.

EXPERIMENTAL

Fig. 1 shows the schematic drawing of 1 cm^2 electrolyzer with double references. H_2 storage Pd reference were placed on the membrane by the contact with 0.5 M H_2SO_4. Anode and cathode electrocatalysts were IrO_x (TKK, ELC-0110) and Pt/C (TKK, TEC10E50E), respectively. The 1.0 mg_{Ir}/cm^2 of anode catalyst was decaled on PEM (Nafion®115, DuPont) with Nafion ionomer, and the 1.0 mg_{Pt}/cm^2 of cathode catalyst was assembled on the membrane as a catalyst coated electrode supported a carbon paper (39BC, SIGRACET®). Two Pt plated Ti (Mitsubishi Materials Corporation, pore size(μm)/porosity(%)/thickness(mm): A_600/84/2.0, B_300/92/2.0) and the carbon

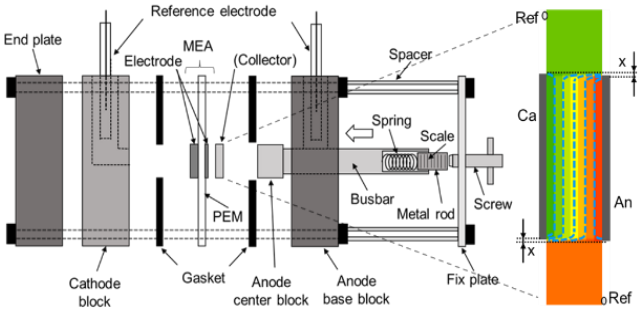

Fig. 1 Electrolyzer structure and MEA arrangement

paper were used as the anode and cathode PTLs, respectively. These electrodes were fixed straight (x = 0 mm) or shift (x = 0.3, 0.5, 0.7, 1.0 mm) stacking as shown in Fig. 1. Operation temperature of the electrolyzer conducted at 80 °C. DI water was pumped and induced at flow rates of 10 ml/min and 2 ml/min to the anode and cathode, respectively. The performance was evaluated by the chronoamperometry (CA) and the electrochemical impedance spectroscopy (EIS).

RESULTS AND DISCUSSION

Fig. 2 shows the relation between the internal resistance R_{ac} obtained from high frequency resistance of EIS and the direct current resistance R_{dc} between two references for the MEAs with various x. The slopes: θ of the lines which passed through the plots and the origin converged to about 0.84 in the range from x = 0.5 to 1.0 mm. This value is used for a correction factor of iR in potential measurements [2].

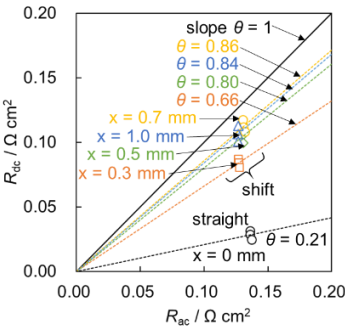

Fig. 2 Relation between R_{ac} and R_{dc}.

Fig. 3 shows the Tafel plots of anode and cathode polarization curves using reference electrodes of anode or cathode sides with x = 1 mm. The R of the iR corrected potential: $E_{corrected}$ was determined 8 % (=(1 - $\theta_{x\ =\ 1}$)/2) of R_{ac}. The $E_{corrected}$ of cathode side was approximately same to the extrapolated Tafel line, so there was almost no mass transfer effect. The reason is that the cathode side was only hydrogen evolution from proton and electrons. Meanwhile, the $E_{corrected}$ of anode side showed excess polarization from the extrapolation of Tafel line above 1.4 V vs. RHE, and especially in the high current density region. It would be affected by larger mass transfer resistance than cathode side. This was considered the water/oxygen transfer resistance or/and the transfer resistance related to the electrons in CL around PTL.

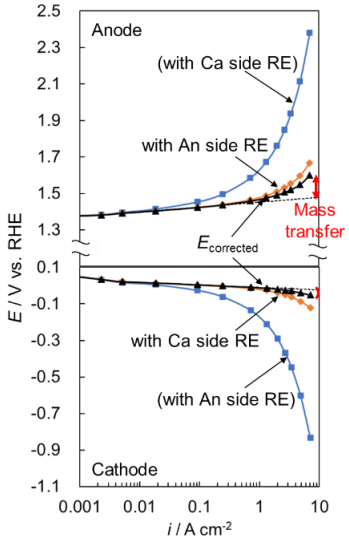

Fig. 3 Separated polarization curves using x = 1.0 mm MEA.

Fig. 4 shows the comparison of mass transfer overpotential for the anode PTL A and B. In this current density range, the overpotential showed the linear relation to the current density. Mass transfer overpotential of the PTL A was as same as half of the PTL B, even we should discuss the determine factor of the mass transfer.

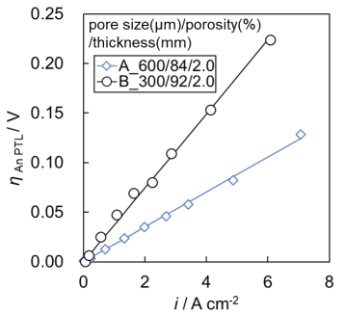

Fig. 4 Comparison of mass transfer overpotential for anode PTLs.

In conclusion, the double references potential measurement with shift arrangement of electrodes enabled to separate the polarization into anode and cathode with iR correction. Based on this method, this measurement method using the developed electrolyzer indicated to be able to evaluate the difference of PTL overpotential for the several type PTLs.

ACKNOWLEDGMENT

This study was partially supported by the development of fundamental technology for advancement of water electrolysis hydrogen production in advancement of hydrogen technologies and utilization project (JPNP14021) commissioned by the New Energy and Industrial Technology Development Organization (NEDO) in Japan.

REFERENCES

[1] M. Carmo, D.L. Fritz, J. Mergel, D. Stolten, Int. J. Hydrogen Energy. 38, 4901-4934 (2013).

[2] YNUセルの参考文献：Int. J. Hydrogen Energy.の投稿中

INVESTIGATION ON METAL OXIDE OXYGEN CARRIERS FOR CHEMICAL LOOPING PROCESSES

KIZILTAN Özge[1], LAMMER Michael[1,2] and HACKER Viktor[1]

[1]Graz University of Technology, Institute of Chemical Engineering and Environmental Technology, Inffeldgasse 25/C, 8010 Graz, Austria, kiziltan@tugraz.at
[2]BEST – Bioenergy and Sustainable Technologies, Inffeldgasse 21, 8010 Graz, Austria

Keywords: Hydrogen production, metal oxide, chemical looping oxygen uncoupling, chemical looping hydrogen

INTRODUCTION

Chemical looping is an emerging technology since it allows for heat generation, hydrogen production and carbon capture [1]. One of the most significant aspects of chemical looping is the development of oxygen carrier materials. The effect of inert support material on carbon deposition for chemical looping hydrogen (CLH) and investigation into a suitable manganese oxide based oxygen carrier for chemical looping with oxygen uncoupling (CLOU) are in the focus of this research.

Carbon deposition is one of the key factors that has to be minimized for high purity hydrogen generation and effective carbon capture and storage. In cyclic operation, previously deposited carbon is reoxidized and produces oxocarbons, which contaminate the product stream [2]. In the recent years, iron oxide is evaluated to be the main oxygen carrier for CLH due to its high oxygen exchange capacity, reaction speed, mechanical resistance, high availability, environmental capabilities and cost effectiveness [3]. During operation at temperatures >800 °C, iron based oxygen carriers are susceptible to sinter effects, leading to a loss of active surface area [4]. Inert high melting metal salts such as aluminum oxide, zirconium oxide and silicon oxide are used as support material to stabilize iron based oxygen carriers. In this study, different support materials are investigated in terms of their contribution to carbon deposition.

Resistance to agglomeration, attrition and fragmentation are desired qualities for oxygen carriers that are to be used for fluidized bed operation [5]. CLUO utilizes two fluidized bed reactors between which oxygen carrier material is circulated [6]. Due to their ability to provide sufficient equilibrium partial pressures of oxygen, manganese oxides and copper oxides are most commonly used for CLUO [4,6]. Since copper has a low melting point of 1075°C [4], it is not desirable for high temperature operation. Manganese based oxygen carriers from different origins are investigated in terms of mechanical strength.

CARBON DEPOSITION

High melting oxides, such as aluminum oxide, silicon oxide, zirconium oxide, titanium oxide and magnesium oxide are utilized as fixed bed in a quartz glass reactor. Carbon deposition is carried out by feeding carbonaceous gasses, e.g. carbon monoxide, to the reactor, as determined by Kuhn et al. [7]. Carbon deposition is followed by gasification step. In this step, oxidizing agents, e.g. steam or synthetic air are fed into the system. The evolved gas is analyzed for carbonaceous species to determine the presence of

carbon deposition. Iron based oxygen carriers with different high melting stabilizers are synthesized by a coprecipitation method. These are characterized in the same way as the pure stabilizing compounds.

CHEMICAL LOOPING OXYGEN UNCOUPLING

In order to be used in a chemical looping oxygen uncoupling process at TU Wien, manganese based oxygen carriers are synthesized from different natural ores and pure manganese oxide by dry mixing, pelletizing and calcination. In previously conducted tests, oxygen carries synthesized from pure manganese oxide showed higher attrition rates and high agglomeration (Fig. 1, left). Oxygen carriers synthesized from manganese ore do not exhibit agglomeration (Fig. 1, right) yet attrition rate is still high. The synthesized oxygen carriers are milled and ground to the desired particle size range for fluidized bed applications. The surface area is measured by mercury intrusion porosimetry. The synthesized oxygen carriers are characterized by thermogravimetric analysis for cyclic behavior and oxygen exchange capacity.

Fig. 1: Oxygen carriers with particle size 180-250 µm, synthesized from pure manganese oxide powder (left) and synthesized from manganese ore (right).

ACKNOWLEDGEMENTS

Financial support by the Austrian Research Promotion Agency (FFG) through the 30th Bridge Call and the project BIO-LOOP within the framework of the COMET - Competence Centers for Excellent Technologies program supported by the Federal Ministry for Climate Action, Environment, Energy, Mobility, Innovation, and Technology (BMK), the Federal Ministry for Digital and Economic Affairs (BMDW), and the Province of Styria (SFG) is gratefully acknowledged.

REFERENCES

[1] T. Mendiara, F. García-Labiano, A. Abad, P. Gayán, L. F. de Diego, M. T. Izquierdo, and J. Adánez, “Negative CO2 emissions through the use of biofuels in chemical looping technology: A review,” Applied Energy, 14-Oct-2018.

[2] S. Bock, “Fixed-bed chemical looping for decentralized hydrogen production and energy storage,” dissertation, Technischen Universität Graz, Graz, Steiermark, 2020.

[3] R. Zacharias, S. Bock, and V. Hacker, “The impact of manufacturing methods on the performance of pelletized, iron-based oxygen carriers for fixed bed chemical looping hydrogen in long term operation,” Fuel Processing Technology, vol. 208, p. 106487, 2020.
[4] R. W. Breault, Handbook of chemical looping technology. Weinheim: Wiley-VCH, 2019.
[5] N. Mohammad Pour, H. Leion, M. Rydén, and T. Mattisson, “Combined cu/mn oxides as an Oxygen carrier in CHEMICAL looping with OXYGEN UNCOUPLING (CLOU),” Energy & Fuels, vol. 27, no. 10, pp. 6031–6039, 2013.
[6] A. Shulman, E. Cleverstam, T. Mattisson, and A. Lyngfelt, “Chemical – looping with Oxygen Uncoupling USING Mn/mg-based Oxygen carriers – Oxygen release and reactivity with methane,” Fuel, 14-Dec-2010.
[7] J. Kuhn and O. Kesler, “Method for in situ carbon deposition measurement for solid oxide fuel cells,” Journal of Power Sources, vol. 246, pp. 430–437, 2014.
[8] M. Luo, Y. Yi, S. Wang, Z. Wang, M. Du, J. Pan, and Q. Wang, “Review of hydrogen production using chemical-looping technology,” Renewable and Sustainable Energy Reviews, 09-Jul-2017.

IEA RESEARCH COOPERATION – ADVANCED FUEL CELLS

LAMMER Michael[1,2], HAMMER Brigitte[1] and HACKER Viktor[1]

[1]Graz University of Technology, Institute of Chemical Engineering and Environmental Technology, Inffeldgasse 25/C, 8010 Graz, Austria, michael.lammer@tugraz.at
[2]BEST – Bioenergy and Sustainable Technologies, Inffeldgasse 21, 8010 Graz, Austria

Keywords: Polymer electrolyte fuel cell, portable applications, international cooperation, transfer of knowledge, IEA topical meeting

INTRODUCTION

The International Energy Agency (IEA) promotes a worldwide research cooperation on important research topics in the energy sector. Its Advanced Fuel Cells Technology Collaboration Programme (AFC TCP) is structured into three technology-type oriented, three application-oriented, an analysis-oriented and a modelling-oriented annex.

The topics covered in this paper include *Annex 31: Polymer Electrolyte Fuel Cells* and *Annex 35: Fuel Cells for Portable Applications*. At the national or international level, analyses are prepared, reports compiled and the associated media work carried out. The results and progress achieved are made available to the IEA, national and international decision-makers, implementation-oriented companies/institutions and the public.

INTERNATIONAL COLLABORATION

Currently, 15 countries are participating in the Technology Collaboration Programme on Advanced Fuel Cells: Austria, China, Denmark, Finland, France, Germany, Israel, Italy, Japan, Mexico, Spain, Sweden, Switzerland, South Korea and the USA.

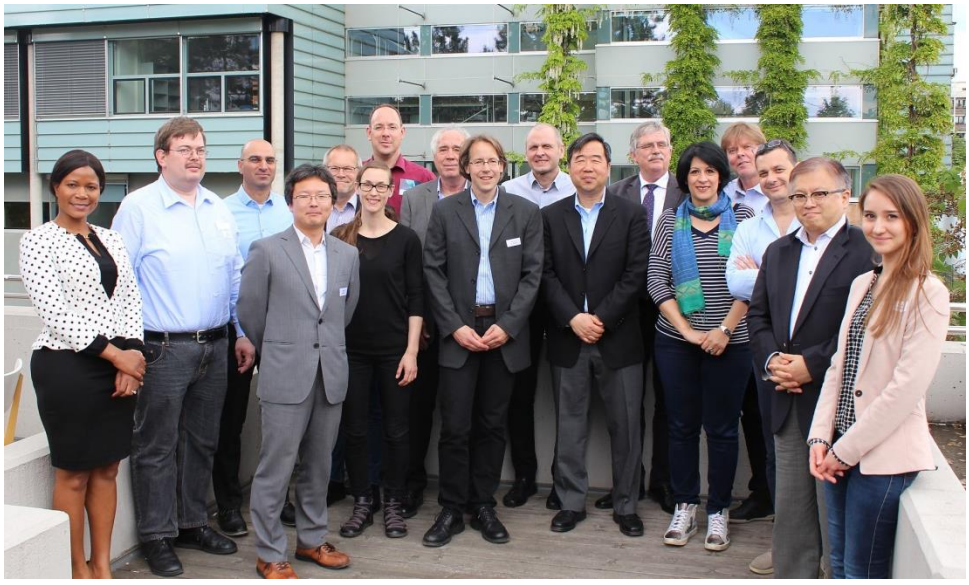

Fig.1: Key participants of the 2017 annex 31 meeting.

Periodic meetings are held to provide information on the results of the research activities and to determine further research work, which is then defined in advance and task-shared in this TCP.The annex 31 meeting was held in 2017 at Graz University of Technology (Fig. 1).

The next topical meeting on *Potential for cost reduction and performance improvement of the IEA AFC TCP for PEMFC at component and system level* will be held as hybrid event at TU Graz and online on 10 and 11 November 2021.

ANNEX 31: POLYMER ELECTROLYTE FUEL CELLS

The Austrian participation is research and development focused. This includes the characterization, evaluation and optimisation of fuel cells as well as the development of materials and techniques to reduce costs and improve performance and lifetime. The systems under consideration include the polymer electrolyte fuel cell (PEFC) and direct fuel cells such as the direct methanol fuel cell (DMFC) and the direct ethanol fuel cell (DEFC), as well as the respective complete systems. The focus is on the following R&D activities:

Characterisation and optimisation of fuel cells

The performance, service life and damage of the cells are determined with specialised test stands for stress test investigations. The thinning of the membrane, the formation of pinholes and the long-term behaviour of fuel cells under load and temperature changes are examined.

Manufacture of membrane electrode assemblies

The use of novel catalyst systems requires new concepts for the production of efficient membrane electrode assemblies. Depending on the viscosity of the catalyst suspension, sedimentation, impregnation and spraying processes are used.

Component and material development

Electrodes and membranes are characterised by means of current/voltage curves, electrochemical impedance spectroscopy and ex situ analysis. Polymetallic catalyst systems are optimised and evaluated using cyclic voltammetry, elemental analysis and electron microscopy.

Fuel conditioning

Innovative processes for the fine purification of the fuel and the influence of trace impurities on the performance of the fuel cells are being evaluated.

ANNEX 35: FUEL CELLS FOR PORTABLE APPLICATIONS

Several fuel cell types are suitable for mobile and portable applications. The focus with regard to use in portable applications is particularly on direct alcohol fuel cells or low-temperature polymer electrolyte fuel cells.

The research activities of the Austrian participation focus on *system, stack and cell development* and *manufacture of membrane electrode assemblies*.

System, stack and cell development

In current projects, the catalytic activity and long-term stability of mono-/bi- or tri-metallic catalysts with regard to ethanol oxidation and oxygen reduction in alkaline media, as well as the performance of membranes, are improved by the addition of functionalised graphene oxide. New anode catalyst systems based on non-precious metals are developed by various selected synthesis methods to achieve controlled homogeneous deposition of catalyst nanoparticles on the support material.

Manufacture of membrane electrode assemblies

The synthesised and further enhanced functionalised graphene-based electrode materials will be used for the development of novel membrane electrode assemblies (MEAs), an evaluation of the influence of production parameters and cell design on the performance of the MEAs and their final characterisation at cell level.

ACKNOWLEDGEMENTS

This project is being conducted within the framework of the IEA research cooperation on behalf of the Federal Ministry for Climate Protection, the Environment, Energy, Mobility, Innovation and Technology.

REFERENCES

[1] IEA Technology Collaboration Programme, Advanced Fuel Cells, annual report 2018/2019. Obtainable online at: https://www.ieafuelcell.com/

[2] M. Lammer, K. Malli, R. Zacharias, A. Jany, K. Kocher, M. Grandi, B. Hammer and V. Hacker: Period report 2017-2019, IEA Fortschrittliche Brennstoffzellen (AFC) Annex 31: Polymerelektrolyt-membran-Brennstoffzellen, Austria, (2020).

[3] V. Hacker: Period report 2014-2017, IEA AFC Annex 31: Fortschrittliche Brennstoffzellen: Polymerelektrolytmembran-Brennstoffzellen, Austria, (2017).

[4] M. Lammer, S. Wolf, B. Cermenek, B. Marius, B. Hammer and V. Hacker: Period report 2017-2019, IEA Fortschrittliche Brennstoffzellen (AFC) Annex 35: Brennstoffzellen für portable Anwendungen, Austria, (2020).

[5] V. Hacker and B. Cermenek: Period report 2014-2017, IEA AFC Annex 35: Brennstoffzellen für portable Anwendungen, Austria, (2017).

FACTORS FOR PROMOTING BUBBLE DETACHMENT FROM ANODES FOR ALKALINE WATER ELECTROLYSIS

MATSUKAWA Kazuyuki[1], IKEDA Hayata[1], KURODA Yoshiyuki[2], MISUMI Ryuta[2] and MITSUSHIMA Shigenori[2,3]

[1]Graduate School of Engineering Science, Yokohama Natl. Univ., 79-5 Tokiwadai, Hodogaya-ku, Yokohama, 240-8501, Japan
[2]Faculty of Engineering, Yokohama Natl. Univ., 79-5 Tokiwadai, Hodogaya-ku, Yokohama, 240-8501, Japan
[3]Institute of Advanced Sciences, Yokohama Natl. Univ., 79-5 Tokiwadai, Hodogaya-ku, Yokohama, 240-8501, Japan
E-mail: cel@ml.ynu.ac.jp

Keywords: Alkaline water electrolysis, Gas bubble, Oxygen evolution reaction, Porous electrode

INTRODUCTION

Toward the realization of a hydrogen society without any carbon dioxide emission, water electrolysis to produce hydrogen using renewable electricity is attracting attention. Alkaline water electrolysis (AWE) is one of the water electrolysis technologies, which uses low-cost materials. To reduce energy consumption of the AWE, the electrolysis bubble around the electrodes, which inhibits mass transfer of reactant and limits the effective electrochemical surface area [1], should be removed effectively. In this study, as a basic evaluation of the effect of bubbles on the polarization of porous electrodes, we have investigated the effect of operation pressure and pore size on apparent activity of oxygen evolution reaction (OER) for Ni porous electrodes.

EXPERIMENTAL

Working electrodes were the Ni Celmet® (Sumitomo Electric Industries, Ltd., pore size of 1.95, 0.85, and 0.51mm, thickness of 3 mm). A counter and a reference were a Ni coil and a reversible hydrogen electrode (RHE), respectively. All measurements were performed with a three-electrode electrochemical cell at 303±1 K with 7.0 M of KOH in a pressurized vessel.

After pretreatment, the effect of pressure on the activity was evaluated with chronopotentiometry for pore size of 0.51 mm electrode in the current range from 50 to 1000 mA cm^{-2}-geo under pressure range from ambient to 0.3 MPa. Also, the effect of pore size on the activity was evaluated with chronoamperometry for mean pore diameter of 1.95, 0.85, 0.51 mm electrodes in the potential range from 1.5 to 2.0 V vs. RHE under ambient pressure. In addition, we observed bubble behavior during electrolysis with the high-speed camera (Photron, FASTCAM Nova S12) in visualized three-electrode electrolyzer under ambient pressure.

RESULTS AND DISCUSSION

Fig. 1 shows the chronopotentiogram as a function of logarithm of time under various pressure at 400 mA cm^{-2}-geo. The visualization of bubble behavior under 0.1 MPa

pressure showed that the bubble formed for 15 ms of electrolysis, because of charging of the electric double layer and dissolving of generated oxygen. After 500 ms of electrolysis, initial bubble detachment began, and the bubble detachment became steady after 1000 ms of electrolysis with increase of potential vibration. Under higher pressure, the trend of the chronopotentiograms was same, but the slopes decreased with the increase of pressure after 15 ms, and the potential increase was also smaller than that of 0.1 MPa.

Fig. 2 shows the steady state polarization curves and the potential increase from 15 to 20000 ms as a function of current of the CPs. The potential decreased with the increase of pressure, simultaneously the potential increase decreased with the increase of pressure. This suggests that pressurization reduced the flow resistance of the bubbles, accelerated their detachment, reduced the bubble volume fraction in the porous medium, and increased the effective surface area of an electrode.

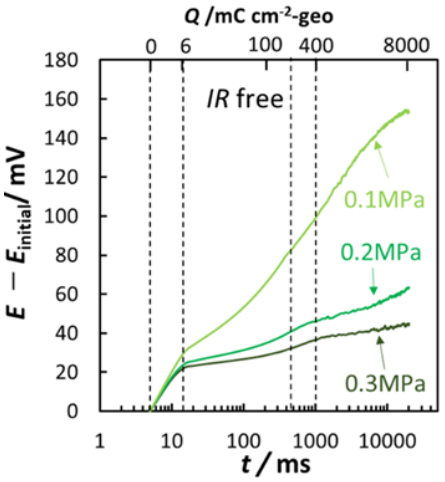

Fig. 1 Potential increase from the start of the CP with 400 mA cm^{-2}-geoas a function of time.

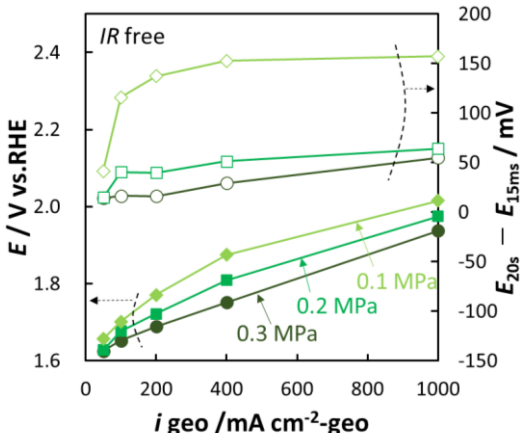

Fig. 2 Polarization curves and potential increase from bubble generation with the anode.

Fig. 3 shows the decrease of current density during the chronoamperometry at 1.8 V vs. RHE as a function of charge passed. The visualization of bubble behavior showed that the timing of bubble generation was about 1, 3, and 7 mC cm^{-2}-geo on the mean pore diameter of 1.95, 0.85, and 0.51 mm electrodes, respectively. Also, the timing of bubble detachment was 50, 90, and 110 mC cm^{-2}-geo. The smaller the pore size electrodes were larger current decrease with later bubble formation. Bubble formation occurs after gas dissolution into the electrolyte on an electrode surface reaches local supersaturation [2]. Supersaturation of a smaller pore size electrode was higher than that of larger pore size one because of larger charge passed before bubble generation. If steady state supersaturation is irrelevant to the pore size, bubble occupancy of smaller pore electrode must become larger than that of larger pore electrode during relaxation period. Fig. 4 shows the polarization curves and the current decrease during bubble generation to detachment as a function of potential. The current decrease increased with the decrease of the pore diameter. This suggests that the flow

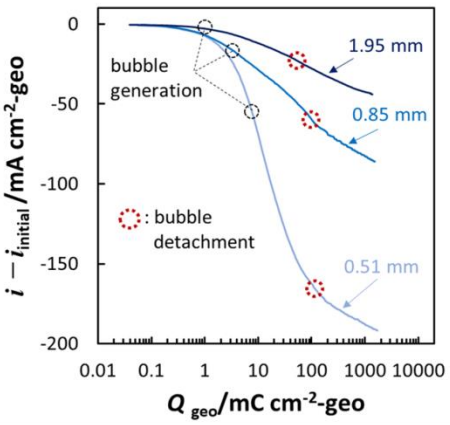

Fig. 3 Current decrease from the start of the 1.8 V vs. RHE as a fuction of Q.

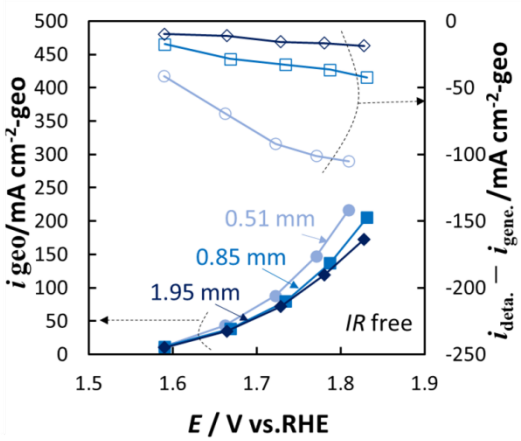

Fig. 4 Polarization curves and current decrease from bubble generation with the anode.

resistance of the bubbles is larger with smaller pore size electrodes, because the pore occupancy of bubble increases with decrease of the pore diameter.

ACKNOWLEDGEMENTS

A part of this study was based on results obtained from the Development of Fundamental Technology for Advancement of Water Electrolysis Hydrogen Production in Advancement of Hydrogen Technologies and Utilization Project (JPNP14021) commissioned by the New Energy and Industrial Technology Development Organization (NEDO).

REFERENCE

[1] S. Marini, P. Salvi, P. Nelli, R. Pesenti, M. Villa, Electrochim. Acta, 82, 384-391 (2012)

[2] M. E. Tawfik, F. j. Diez, Electrochim. Acta, 146, 792-797 (2014)

DESIGN AND CONTROL OF A LAB SCALE HUMIDIFICATION SYSTEM FOR PEFC

MAYR Niklas, FITZ Manuel, MARIUS Bernhard and HACKER Viktor

TU Graz, Institute of Chemical Engineering and Environmental Technology, Inffeldgasse 25/C, 8010 Graz, Austria, Austria, niklas.mayr@student.tugraz.at

Keywords: two phase bubble humidification system, regulation, PEMFC

INTRODUCTION

This paper presents an improved design of the commonly used bubble humidifiers and an approach to control the relative humidity of the reaction gases.

SPECIFICATION & CHARACTERISATION OF THE HUMIDIFIER SYSTEM

I n Fig. 1 the humidifier, its dimensions and the control elements are shown. The liquid and gas phase are heated with two separate heating cables with Pt-100 thermocouples in the respective phase (TIC-01 and TIC-02). The temperature of the gas phase is measured at the outlet of the humidifier while the temperature of the liquid phase is measured in the middle of the water phase. In the bottom section two perforated plate spargers are mounted to accommodate a Raschig® rings filling. The filling and the sparger plates disperse the gas flow and thereby increase the specific surface area for a better mass transfer by limiting the maximum bubble size. [3]

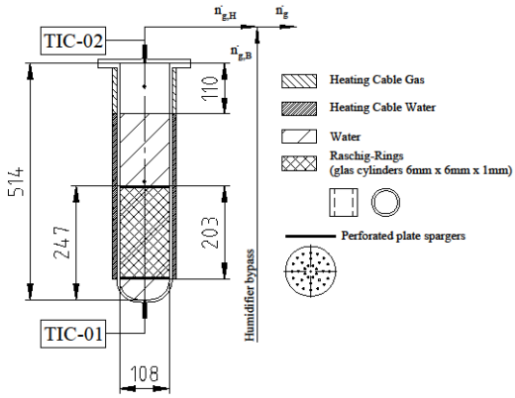

Fig. 1: Design specifications of the humidifier, its internals and measurements.

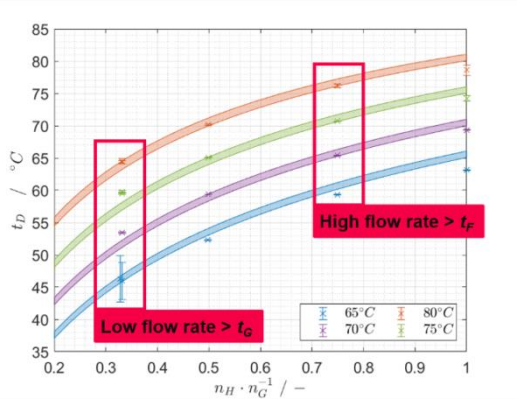

Fig. 2: The temperature at the dew point at different temperatures of the humidifier and ratios of the $\dot{n}_{g,H}$ and the $\dot{n}_g$.

After the humidifier the gases are superheated to prevent condensation. For long term tests the humidifiers are regularly refilled with preheated water using liquid mass flow controllers. The amount of water refilled is calculated based on the continuously measured dry gas flow and the measured humidity after the humidifier.

A thermodynamic model is derived based on the assumption of ideal gas and ideal mixture. The Magnus equation and parameters of Wiegleb [4] are used for calculating the vapour pressure of water. Based on this assumption the dew point temperature of the reactant gas can be calculated as a function of the temperature of the humidifier and the flow rates through the humidifier and the bypass. Since the gas phase is tempered 1 °C above the temperature of the liquid phase the model is displayed as an area in Fig. 2. The model and the measured data are in qualitative and quantitative agreement.

REGULATION

The dew point of the reactant gases is regulated by adjusting the flow of dry gas through the bypass n˙_(g,B) and the flow of humidified gas through the humidifier n˙_(g,H). To maintain the required stoichiometry the total gas flow n˙_g is kept constant. A dimensionless, virtual regulation variable x shown in equation 1 is introduced and regulated with a PID regulator. [5]

$$x \overset{\text{def}}{=} \frac{\dot{n}_{g,H}}{\dot{n}_{g,H}+\dot{n}_{g,B}} \quad \Rightarrow \quad \dot{n}_{g,H} = \dot{n}_g x \quad and \quad \dot{n}_{g,B} = n_g(1-x) \tag{1}$$

A step response from x = 0 □(→┬step) x=1, which corresponds to ϕ = 0 □(→┬step) ϕ =50 %RH at 78 ° C humidifier temperature is used to calculate four different parameter sets according to the T_Σ scheme. [6] The dynamic behaviour is characterised by the maximum overshoot and the duration until the accuracy of ±0.5 %RH is reached while the stationary behaviour of the system is characterised with the standard deviation of the last two minutes of the respective test.

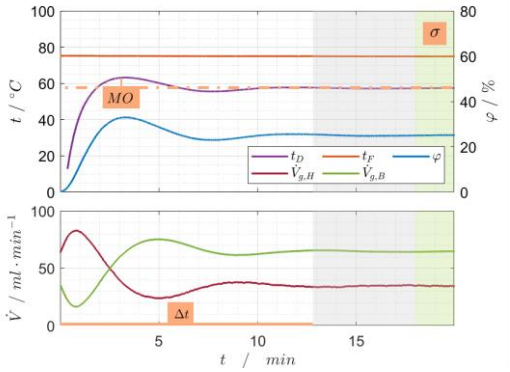

Fig. 3: Regulation characteristics: maximum overshoot MO, duration until the required accuracy is reached Δt and standard deviation of the stationary behaviour σ.

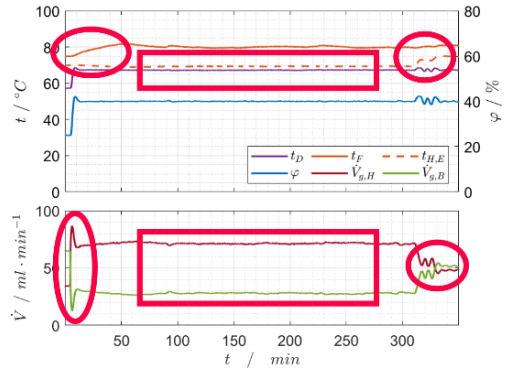

Fig. 4: Suppression of system disturbances by the controller. Right: Oscillations of the set point and the system response to investigate the dynamic behaviour of the system.

In Table 1 the regulation characteristics are stated for the investigated regulation parameters as well as some exemplary states. The PID_Fast yields the smallest overshoot and has the highest accuracy in the stationary phase. Thus it is recommended to use this parameter set. To validate the stability of the developed regulation system, it has been tested at different temperatures of the humidifier and for

different dew point set points. Further it was shown that the system can suppress external disturbances like an unstable temperature of the humidifier.

Table 1: Regulation characteristics of the investigated parameter sets and their application for different system states. [7]

Evaluation of PID Parameters					Evaluation of different States				
Unit	φ_{set} %	Δt min	MO %	σ $\% \cdot 10^{-2}$	t_H $°C$	φ_{set} %	Δt min	MO %	σ $\% \cdot 10^{-2}$
PI_{slow}	40	9.97	7.03	3.73	75	25	12.81	7.97	6.62
PID_{slow}	40	9.69	6.20	5.48	80	40	10.56	11.50	10.02
PI_{fast}	40	8.98	6.14	4.44	80	55	13.82	3.31	4.19
PID_{fast}	40	9.92	4.41	3.40					

CONCLUSION

The improvements in the bubble humidifier of the fuel cell test, lead to a stable and reproducible humidification of the fuel cell. Condensation of steam is effectively prevented by tempering the gas phase 1 °C above the temperature of the liquid phase.

By controlling the flow through the bypass and humidifier, accurate measurements of the PEFC can be made because (a) the humidity of the reaction gases is kept exactly constant or (b) the effects of humidity changes on fuel cell performance can be studied. Specifically, a humidity set point can be set within 13 min with an accuracy of ±0.5 %RH. This makes it more than ten times faster than conventional humidifier temperature control, which typically requires ~2 h to achieve an accuracy of ±2.5 %RH. Simultaneously fluctuations due to an unstable humidifier temperature can be effectively suppressed.

REFERENCES

[1] Hacker, V., Mitsushima, S., 2018: Fuel cells and hydrogen: from fundamentals to applied research, Elsevier.

[2] Chen, H., Pei, P., Song, M., 2015: Lifetime prediction and the economic lifetime of Proton Exchange Membrane fuel cells, Applied Energy, 142, 154 – 163.

[3] Ranz, M., 2019: Die Kontrolle der Gasfeuchte und deren Auswirkung auf die Performance einer Brennstoffzelle, TU Graz, Institute of Experimental Physics.

[4] Wiegleb, G., 2016: Gasmesstechnik in Theorie und Praxis: Messgeräte, Sensoren, Anwendungen, Springer-Verlag.

[5] Raman, S., Swaminathan, S., Bhardwaj, S., Tanneru, H. K., Bullecks, B., & Rengaswamy, R. (2019). Rapid humidity regulation by mixing of dry and humid gases with feedback control for PEM fuel cells. International Journal of Hydrogen Energy, 44(1), 389-407.

[6] Kuhn, U., 1995: Eine praxisnahe Einstellregel f¨ur PID-Regler: Die T-Summen-Regel, Automatisierungstechnische Praxis, 37(5), 10–16.

[7] Mayr, N., 2020: Characterization and Regulation of Gas Humidification Systems for Polymer Electrolyte Fuel Cells at Laboratory Scale, TU Graz, Institute of Chemical Engineering and Environmental Technology

STRUCTURE AND ACTIVITY OF ELECTROLYTICALLY DEPOSITED HYBRID COBALT HYDROXIDE NANOSHEETS FOR SELF-REPAIRING OXYGEN EVOLUTION REACTION CATALYSTS

NAKAJIMA Ritsuki[1], TANIGUCHI Tatsuya[2], OISHI Ayaka[2], NAGASHIMA Ikuo[2], INOMATA Akihiko[2], NISHIKI Yoshinori[3], AWALUDIN Zaenal[3], NAKAI Takaaki[3], KATO Akihiro[3], MITSUSHIMA Shigenori[1,4] and KURODA Yoshiyuki[1,4]

[1]Grad. School of Eng. Sci., Yokohama Natl. Univ., 79-5 Tokiwadai, Hodogaya-ku, Yokohama 240-8501, Japan
[2]Kawasaki Heavy Ind., Ltd., 1-1 Kawasakicho, Akashi, Hyogo, 673-8666, Japan
[3]De Nora Permelec, Ltd., 2023-15 Endo, Fujisawa, Kanagawa, 252-0816, Japan
[4]Adv. Chem. Energy Res. Center, Inst. of Adv. Sci., Yokohama Natl. Univ., 79-5 Tokiwadai, Hodogaya-ku, Yokohama 240-8501, Japan
E-mail: cel@ml.ynu.ac.jp

Keywords: Alkaline water electrolysis, Self-repairing catalyst, Oxygen evolution reaction

INTRODUCTION

Water electrolysis is a core technology in the conversion of renewable energy to hydrogen. Alkaline water electrolysis (AWE) is one of the most suitable technologies because of its low cost and applicability to large-scale production of hydrogen. However, the AWE system exhibits electrode degradation under fluctuating electricity from renewable energy. Recently, we have demonstrated the use of a hybrid cobalt hydroxide nanosheet (Co-ns) to form a self-repairing catalyst layer on a nickel anode under cycled potential [1], although formation process of catalyst layer and factors affecting the oxygen evolution reaction (OER) are not sufficiently understood. In this study, we investigated the catalyst formation process and activity via different deposition methods.

EXPERIMENTAL

Co-ns was synthesized according to the literature [2]. Electrochemical tests were performed in a 1.0 M KOH, using a PFA three-electrode cell. A nickel plate, a nickel coil, and a reversible hydrogen electrode were used as the working, counter, and reference electrodes, respectively. For pre-treatment, the surface Ni oxide/hydroxide was electrochemically removed by at −0.5 V vs. RHE. The Co-ns dispersion (final concentration 40 ppm) was then added in the electrolyte. Co-ns was deposited by the two protocols. Cycled method is according to our previous report [1]. The following processes were repeated for 8 or 30 times: i) chronopotentiometry (CP) at 800 mA cm^{-2} for 30 min, ii) cyclic voltammetry (CV) between 0.5 and 1.8 V vs. RHE at 5 mV s^{-1}, iii) CV between 0.5 and 1.6 V vs. RHE at 50 mV s^{-1}, iv) electrochemical impedance spectroscopy (EIS) at 1.6 V vs. RHE with the frequency range $0.1-10^5$ Hz. The following deposition protocol, called the continuous method, was newly employed, where CP at 800 mA cm^{-2} for 4 or 15 hours was performed, followed by the above processes ii−iv once.

RESULTS ANS DISCUSSION

The electrode prepared by the continuous method exhibited higher OER activity than those prepared by cycled method. The $Co^{2+/3+}$ redox peaks appeared at different potential, suggesting a change in the composition and/or crystal structure (Fig. 1). The charge of the anodic peaks due to $Co^{2+/3+}$ (Q_a) was used as a measure of the amounts of the deposited Co-ns.

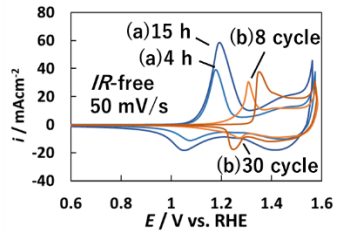

Fig. 1 Polarization curves of the Co-ns-coated Ni electrodes at 50 mV s^{-1}. Experimental conditions：(a) the continuous method, (b) the cycled method.

The current density at 1.6 V vs. RHE ($i_{1.6V}$) exhibited a linear relationship with Q_a by the continuous method (Fig. 2). Indicating that the catalytic activity is proportional to the amount of the deposited Co-ns. By the cycled method, the plots appeared on the same line as those obtained by the continuous method. Q_a was monotonically increased up to the 15th cycle, whereas it turned to decrease after the cycle. Therefore, the OER activity depends hardly on the structure but on the amount of deposited Co-ns.

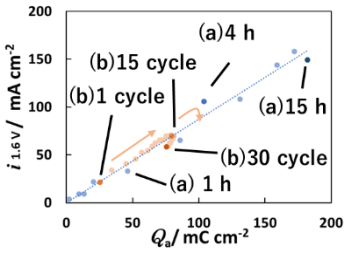

Fig. 2 The current density at 1.6 V vs. RHE as a function of anode peak electric quantity. Experimental conditions：(a) the continuous method, (b) the cycled method.

To investigate the relationship between the morphology of the catalyst film and Q_a, $i_{1.6V}$ was plotted over the coverage of the electrode surface with Co-ns, estimated by the EDS mapping (Fig. 3). The coverage increased after longer electrolysis by the continuous method together with the increase in the OER activity. Contrary, the coverage reached 88% at the 8th cycle and decreased to 71% at the 30th cycle by the cycled method, indicating that a part of the catalyst layer was dissolved/delaminated during the process. The surface of the catalyst layer by the continuous method was flat, though that by the cycled method was rough, being consistent with the decrease in Q_a. Thus, potential sweep probably affects the dissolution or delamination of the catalyst layer, causing the decrease in the activity. Interestingly, $i_{1.6V}$ still increased along with the electrolysis time after the increase in the coverage finished, suggestion that the active sites distribute not only on the surface of the catalyst layer but also inside the layer.

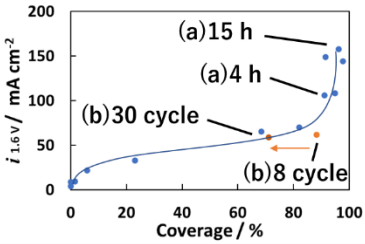

Fig. 3 The current density at 1.6 V vs. RHE as a function of the catalyst coverage. Experimental conditions：(a) the continuous method, (b) the cycled method.

In conclusion, it was found that the OER activity of the Co-ns catalyst layer depends on the amount of deposited Co-ns and potential sweep during the catalyst deposition process causes partial dissolution/detachment and decrease in the activity. These insights will contribute to achieve both higher activity and higher durability for self-repairing catalysts.

ACKNOWLEDGEMENTS

This work was supported partially by the JSPS KAKENHI from MEXT, Japan.

REFERENCES

[1] Y. Kuroda, T. Nishimoto, S. Mitsushima, Electrochim. Acta, 323, 13481 (2019).
[2] Y. Kuroda, T. Koichi, K. Muramatsu, K. Yamaguchi, N. Mizuno, A. Shimojima, H. Wada, K. Kuroda, Chem. Eur. J., 23, 5023 (2017).

EVALUATION OF ELECTRODE MATERIAL CHARGE/DISCHARGE CHARACTERISTICS FOR ALKALINE WATER ELECTROLYSIS AND EXAMINATION OF ITS EFFECT ON REVERSE CURRENT

ODA Kazuaki[1], KURODA Yoshiyuki[1,2] and MITSUSHIMA Shigenori[1,2]

[1]Grad. School of Eng. Sci., Yokohama Natl. Univ., Japan.
[2]Inst. Adv. Sci., Yokohama Natl. Univ., Japan.

Keywords: Alkaline Water Electrolysis, Reverse current, Anode, Durability.

INTRODUCTION

In alkaline water electrolysis (AWE), the generation of reverse current due to charging and discharging of the electrodes becomes a problem when electrolysis is stopped [1]. Materials such as catalysts and intermediate layers are often composited for water electrolysis electrodes, and it is necessary to analyze the contribution of each constituent material to the reverse current individually. There are few reports on charge/discharge behavior under AWE conditions. In this report, we conducted charge/discharge tests of the anode for AWE, and collected and examined basic data on how each material behaves when electrolysis is stopped.

EXPERIMENT

Catalyst Preparation

α-Mn_2O_3 : $Mn(NO_3)_2 \cdot 6H_2O$ was heated at 800 °C for 1 h.

Co_3O_4 : $Co(NO_3)_2 \cdot 6H_2O$ was heated at 800 °C for 1 h.

$MnCo_2O_4$: The mixture of $Mn(NO_3)_2 \cdot 6H_2O$(1 mmol) and $Co(NO_3)_2 \cdot 6H_2O$(2 mmol) was heated at 800 °C for 1 h.

$CoMn_2O_4$: The mixture of $Co(NO_3)_2 \cdot 6H_2O$(1 mmol) and $Mn(NO_3)_2 \cdot 6H_2O$(2 mmol) was heated at 800 °C for 1 h.

$NiCo_2O_4$: The mixture of $Ni(NO_3)_2 \cdot 6H_2O$(1 mmol) and $Co(NO_3)_2 \cdot 6H_2O$(2 mmol) was heated at 800 °C for 1 h.

α-MnO_2 : The mixture of $Mn(OAc)_2 \cdot 4H_2O$(9 mmol)and $KMnO_4$(6 mmol) was heated at 120 °C for 4 h.

$CoMnO_3$: The mixture of $Co(NO_3)_2 \cdot 6H_2O$(1 mmol) and $Mn(NO_3)_2 \cdot 6H_2O$(1 mmol) was heated at 500 °C for 1 h.

$NiMnO_3$: The mixture of $Ni(NO_3)_2 \cdot 6H_2O$(1 mmol) and $Mn(NO_3)_2 \cdot 6H_2O$(1 mmol) was heated at 500 °C for 1 h.

Electrochemical Measurements

All of the electrochemical measurements were performed in a three electrode system made by PTA. Working Electrode(WE) was prepared as follows; the catalyst(40 mg),

Acetylene Black(5 mg), 8%PVdF(62.5 mg) and NMP(100 uL) were well mixed and casted on Ni plate(1.0 cm×1.5 cm).Finally, this as-prepared catalyst was vacuum dried at 60 °C (1 h) and 120°C (1 h) subsequently. RHE(Pt, H_2 atmosphere) is used as Reference Electrode(RE), Ni Coil is used as Counter Electrode(CE).

Cyclic Voltammetry(CV) and Charge/Discharge test was carried out in 1 M KOH solution(N_2 atmosphere, 25 °C). CV was conducted with a scan rate of 10 mV s^{-1} from 0.5 to 1.8 V vs. RHE before/after Charge/Discharge test. Charge/Discharge test was conducted from 1.5 V to 0.5 V vs. RHE with a cycling rate of 500 uAcm^{-2}. This process was repeated 10 times.

RESULTS AND DISCUSSION

Fig. 1 showed all XRD patterns, in α -MnO_2, $CoMnO_3$ and $NiMnO_3$ pattern, these peaks were very broad. The others which made at high temperature(500℃,800℃) had sharp XRD patterns. Scherrer's equation was used to calculate particle size from this graph.

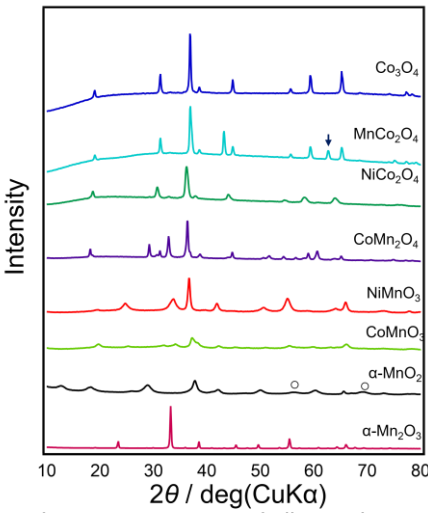

Fig. 1 XRD patterns of all samples

Fig. 2 showed discharge capacity of all samples and cycles. α-MnO_2, $CoMnO_3$, $NiMnO_3$ showed over 40mAh g^{-1} discharge capacity at first cycle. These catalysts showed relatively high capacity under AWE condition. 10th discharge capacity of α-MnO_2 decreased 53% and 14% increase and 17% decrease was confirmed from $CoMnO_3$ and $NiMnO_3$ respectively. CV graphs of these three samples turned into a same type of CV graphs after 10 cycles. On the other hand, Spinel type structure catalysts (Co_3O_4, $MnCo_2O_4$, $CoMn_2O_4$, $NiCo_2O_4$) and α-Mn_2O_3 showed small discharge capacity under 4 mAh g^{-1} at first cycle and these catalysts kept their first capacity. CV graphs of these samples were almost same graph before/after Charge/Discharge test.

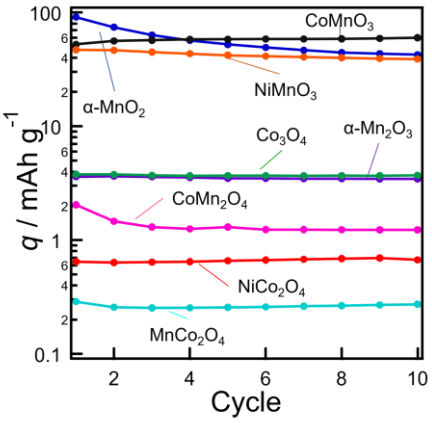

Fig. 2. Discharge capacity as a function of charge/discharge cycles.

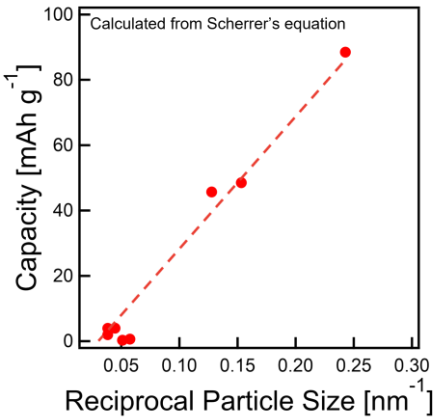

Fig. 3.1st Discharge capacity as a function of reciprocal of particle size.

Catalyst made at high temperature had large particle size and high cycle stability. Relation between first capacity and reciprocal particle size was investigated since specific surface area is proportional to reciprocal particle size (Fig.3). This implies that Charge/Discharge reaction was occurred only sparse surface area of catalysts. Crystallinity is considered to be an important factor contributing to stability because specific surface area well affects cyclic stability of catalysts. However, there was no clear relations among catalyst which has tiny reciprocal particle size (under 0.1[nm^{-1}]).

From these facts, Charge/Discharge reaction was mainly happened on only sparse surface area and affects capacity. This result could be a material for determining the optimum particle size based on the surface area dependence of the activity.

REFERENCES

[1] Y. Uchino, et. al. Electrocatalysis. 9 (2018), p. 67-74

CONTROL OF WATER TRANSPORTATION IN DIRECT TOLUENE ELECTRO-HYDROGENATION ELECTROLYZER

OI Shota[1], NAGASAWA Kensaku[2], TAKAMURA Toru[3], MISU Yoshitatsu[3], MATSUOKA Koji[3] and MITSUSHIMA Shigenori[1,2]

[1]Graduate School of Engineering Science, Yokohama National University, 79-5 Tokiwadai, Hodogaya-ku, Yokohama 240-8501, Japan
[2]Institute of Advanced Sciences, Yokohama National University, 79-5 Tokiwadai, Hodogaya-ku, Yokohama 240-8501, Japan
[3]Central Technical Research Laboratory, ENEOS Corporation, 8 Chidoricho, Naka-ku, Yokohama 231-0815, Japan
E-mail: cel@ml.ynu.ac.jp

Keywords: Direct toluene electro-hydrogenation, Water transport, Electro-osmotic coefficient, Back diffusion

INTRODUCTION

To decrease carbon dioxide emissions, utilization of renewable energy must be major primary energy source. Therefore, the large-scale storage and transportation of hydrogen as secondary energy is needed for effective utilization of fluctuated and unevenly distributed renewable energy. Toluene (TL) / methylcyclohexane (MCH) organic hydride system is one of the best candidates of hydrogen energy carrier, because TL and MCH are liquid at ambient temperature and pressure, and it would be able to use petroleum infrastructure. To improve the energy conversion efficiency for TL hydrogenation using renewable electricity, we have studied direct electro-hydrogenation of TL with water decomposition using proton exchange membrane (PEM). The rate-determining step for the cathode is the mass transfer of TL to the catalyst layer [1]. One of the major factors inhibiting TL transportation to the cathode catalyst is electro-osmotic drag water from the anode through the membrane. The accumulation of the water in the catalyst layer inhibits the TL transportation and decreases the current efficiency, but its behavior has not been clarified. In this study, the influence of current density, sulfuric acid concentration of anolyte and cell temperature on water flux through the membrane were evaluated to control the water transportation in direct TL electro-hydrogenation electrolyzer.

EXPERIMENTAL

A DSE® (De Nora Permelec, Ltd.) for the oxygen evolution and Nafion 117® (Du Pont) were used as the anode and PEM, respectively. Carbon paper (10BC, SGL carbon ltd.) loaded with 0.5 mg-PtRu cm^{-2} of PtRu/C (TEC61E54, Tanaka Kikinzoku Kogyo) was used as the cathode. The carbon paper, which also serves as the cathode flow channel, was preloaded with 0.02 mg cm^{-2} of Pt catalyst for chemical hydrogenation by impregnation method. The cathode was hot-pressed on the PEM at 120 ^{o}C and 15 MPa for 3 min to fabricate a membrane cathode assembly.

The anode and cathode compartments were circulated 0-1.5 M (= mol dm^{-3}) H_2SO_4 and 10% TL/MCH, respectively. Operation temperature of the electrolyzer conducted at 50-

80 °C. As the electrochemical measurement, chronopotentiometry at 0.1-0.4 A cm^{-2} was conducted for 20 min, and the water amount through the membrane was evaluated by measuring the weight of it in the reservoir after electrolysis. The concentration of sulfuric acid of the water was determined by measuring the pH.

RESULTS AND DISCUSSION

The water flux through the PEM by electro-osmosis and diffusion is given by eq. (1) [2]. The physical quantities in eq. (1) are listed in Table 1.

$$J_{\mathrm{H_2O}} = M_{\mathrm{H_2O}} \left(n \frac{i}{F} - D_{\mathrm{w}} \frac{da_{\mathrm{w}}}{dx} \right) \qquad (1)$$

If water flux has linear relation to current density would mean the water flux function of eq. (1) with constant apparent electro-osmotic coefficient: *n* and constant back diffusion term. The constant back diffusion would mean that constant activity of aqueous phase forms in the cathode catalyst layer.

Table 1: Physical quantities controlling the water flux

Symbol for quantity	Physical quantity
$J_{\mathrm{H_2O}}$	Water flux
$M_{\mathrm{H_2O}}$	Molecular weight of water
n	Electro-osmotic coefficient
i	Current efficiency
F	Faraday constant
D_{w}	Diffusion coefficient of water
$\frac{da_{\mathrm{w}}}{dx}$	Activity gradient of water

Fig. 1 shows dependence of cell voltage and water flux at 60 °C with various sulfuric acid concentrations on current density. There was no significant difference in cell voltages except for 0 M. The relationship between the water flux and the current density were linear except 0.1 A cm^{-2} at 1.5 M. The water flux decreased as the sulfuric acid concentration increases except for 0 M. The absolute value of the intercept by extrapolating the linear region increased with sulfuric acid concentration increase. The slope of the linear region decreased with the sulfuric acid concentration increase. In addition, the water phase in the cathode compartment was sulfuric acid whose concentration was about one-tenth that of the anolyte. The sulfuric acid would impregnate into the membrane and its concentration would be a continuous function in the through-plane direction of the membrane.

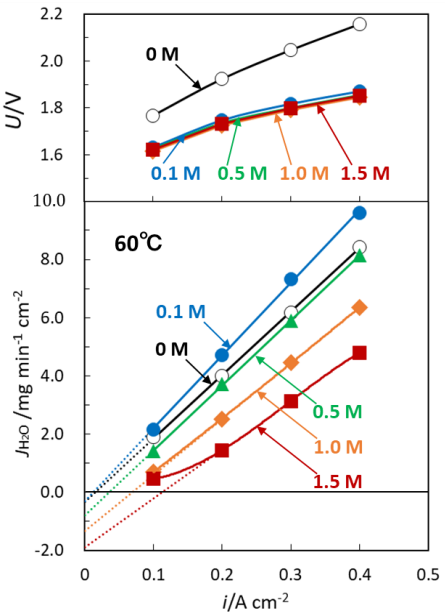

Fig. 1. Dependence of cell voltage and water flux at 60 °C with various sulfonic acid concentrations on current density.

Fig. 2 shows dependence of apparent electro-osmotic coefficient and back diffusion term on sulfuric

acid concentration. The apparent electro-osmotic coefficient and the back diffusion term were determined by the slope and the intercept of Fig. 1, respectively. They had linear relation to the anolyte concentration except for 0 M. The local electro-osmotic coefficient would decrease with increase of the local sulfuric acid concentration in the membrane, and the apparent electro-osmotic coefficient had decreased linearly with increase of the anolyte concentration because of impregnation of sulfuric acid into the membrane. The back diffusion term, which is affected by the sulfuric acid concentration difference, increased linearly with anolyte concentration increase. Both of them would be explained with impregnated sulfuric acid concentration in the membrane.

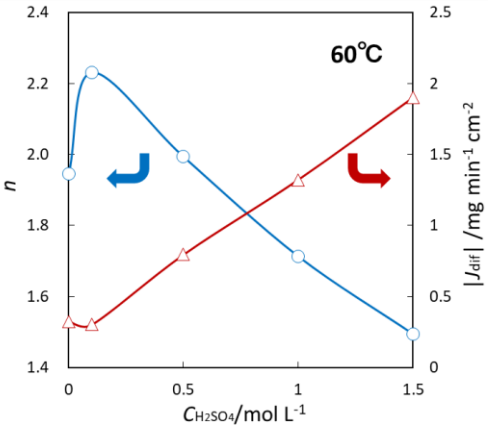

Fig. 2: Dependence of apparent electro-osmotic coefficient and back diffusion term on sulfuric acid concentration.

ACKNOWLEDGEMENTS

This work was supported by the Toyota Mobility Foundation. Anode was supplied by De Nora Permelec Ltd. We appreciate the person concerned them.

REFERENCES

[1] K. Nagasawa, Y. Sawaguchi, A. Kato, Y. Nishiki, S. Mitsushima, Electrocatalysis, 8, 164 (2017).
[2] T. E. Springer, T. A. Zawodzinski, S. Gottesfeld, J. Electrochemical Society, 138, 2334 (1991).

THE EFFECT OF ULTRAFINE-BUBBLE ON ELECTRODE REACTION FOR ALKALINE WATER ELECTROLYZER

OZAWA Ryo[1], KURODA Yoshiyuki[1,2] and MITSUSHIMA Shigenori[1,2]

[1]Graduate School of Engineering Science, Yokohama National University, 79-5 Tokiwadai, Hodogaya-ku, Yokohama 240-8501, Japan.
[2]Institute of Advanced Sciences, Yokohama National University, 79-5 Tokiwadai, Hodogaya-ku, Yokohama 240-8501, Japan.
E-mail: cel@ml.ynu.ac.jp

Keywords: Water electrolysis, Ultrafine Bubble, Hydrogen evolution reaction

INTRODUCTION

Green hydrogen, hydrogen produced without the emission of CO_2, has attracted much attention to resolve global warming. Water electrolysis is one of the promising technologies for hydrogen production from renewable energy. One of the major issues in water electrolysis is that blocking of electrode surface by generated bubbles. Quick removal of bubble from electrode is highly demanded to develop more efficient electrolyzers. An ultrafine bubble (UFB) is a bubble with a diameter of 1 μm or less. Because it has been reported that UFBs decrease viscosity and surface tension of the solution [1], it is expected that UFBs in an electrolyte of a water electrolyzer accelerates the detachment of bubbles. In this study, we investigated the influence of UFB to the kinetics of hydrogen evolution reaction (HER) and analyzed the hydrogen bubbles generated by HER.

EXPERIMENTAL

HER was carried out using a general three-electrode cell. As electrolytes, 0.1 M H_2SO_4 and 1 M KOH were investigated. To prepare the electrolytes contining UFBs, UFBs were first generated in deionized water by the pressurized dissolution method (circulation: 50 times,0.2Mpa). The UFB-containing water was then diluted with 1 M H_2SO_4 or 10 M KOH to obtain H_2SO_4-UFB and KOH-UFB, respectively. Electrolytes without UFBs are denoted as H_2SO_4 and KOH. Pt wire was used as the working electrode in H_2SO_4 and H_2SO_4-UFB and Ni wire in KOH and KOH-UFB. Cyclic voltammetry (CV) was performed between –1.0 V and 0.1 V vs. RHE at 5 mV/s. The solution resistance for the *iR* correction was measured by the electrochemical impedance spectroscopy.

UFBs generated by the HER was investigated as follows. An electrolytic cell equipped with Ni coil (anode) and Ni mesh (cathode, 16 cm^2) separated by Nafion was filled with 1 M KOH or 0.1 M Na_2SO_4 as an electrolyte (200 cm^3). Constant current electrolysis at 30 mA/cm^2 for 10minute was applied to generate hydrogen from the cathode side. The electrolyte on the cathode side was collected and allowed to stand, and the particle size and concentration of the internal particles were measured by the laser diffraction.

RESULTS AND DISCUSSIONS

Fig. 1 shows the Tafel plots of HER in H_2SO_4 (a) and KOH (b). The linear Tafel region is expected to be charge-transfer limiting, whereas non-linear region shoudl be affected by the mass transport due to blocking of electrode surface by the generated H_2 bubbles. When H_2SO_4 is used as an electrolyte, the upper limit current density of the linear Tafel region is increased by adding UFBs in the electrolyte. It suggests mass transport becomes rate-limiting is larger with UFB-H_2SO_4. This suggests that the addition of UFB accelerates the desorption of the generated bubbles. On the other hand, when KOH is used as an electrolyte, no change was observed in the Tafel plots. Therefore, the influence of the added UFB is very small in alkaline electrolyte.

To understand more on the alkaline electrolyte, UFBs generated by HER in the neutral and alkaline electrolytes were investigated. Fig. 2 shows the particle size and concentration of particles present in the electrolyte after the electrolysis. Because the concentration of bubbles decreased day by day and the particle size remained in the range of 100-200 nm, the existing particles are attributable to UFBs. The concentration of UFBs in the KOH electrolyte was more than five times than those in the Na_2SO_4 electrolyte. In addition, the UFBs in the KOH electrolyte had longer lifetime than those in the Na_2SO_4 electrolyte. According to the literature on the non-electrolytic UFBs, UFBs are more stable in solutions with higher pH because hydroxide ions are adsorbed on the surface of UFBs [2]. This should be common for electrolytic UFBs. Because much UFB is generated in an alkelaine electrolyte by electrolysis, it is thought that the additional UFBs afffect less on the HER kinetics.

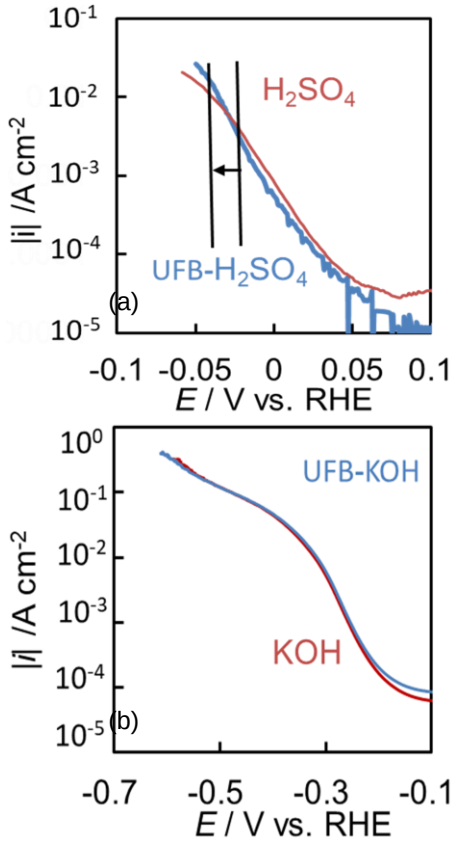

Fig.1. Comparison of polarization curves of H_2SO_4 (a) and KOH (b) with and without UFB during hydrogen evolution reaction

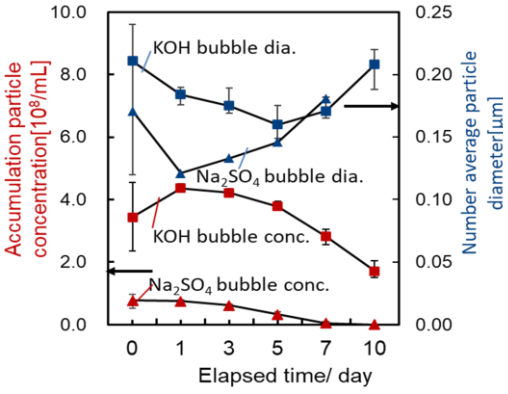

Fig.2. Changes in particle size and concentration in solution after electrolysis

REFERENCE

[1] P. Attard, Eur Phys J Spec Top, 223, 893 (2014).
[2] K. Shuo, W. Xiao, N. Quan, Y. Dong, L. Zhang, J. Hu, Langmuir, 35, 5250, (2019)

SURFACE CHARACTERIZATION OF ELECTRODES USED IN ALKALINE DIRECT ETHANOL FUEL CELLS

ROSCHGER Michaela, WOLF Sigrid and HACKER Viktor

TU Graz, Institute of Chemical Engineering and Environmental Technology, Inffeldgasse 25/C, 8010 Graz, Austria, michaela.roschger@tugraz.at, viktor.hacker@tugraz.at

Keywords: alkaline direct ethanol fuel cell, electrode characterization, scanning electron microscopy, polarization curve.

INTRODUCTION

In alkaline direct ethanol fuel cells (ADEFCs), shown in Fig. 1, the carbon-neutral fuel ethanol is theoretically oxidized to CO_2 and water. The incomplete conversion to acetate is one of the barriers (ethanol crossover, mixed potentials, homogeneous distribution of the catalysts on the electrodes), which must be solved before its commercialization. However, it also stands out for its great advantages: easy storage and transport, low toxicity, its robustness, environmental friendliness and low costs [1].

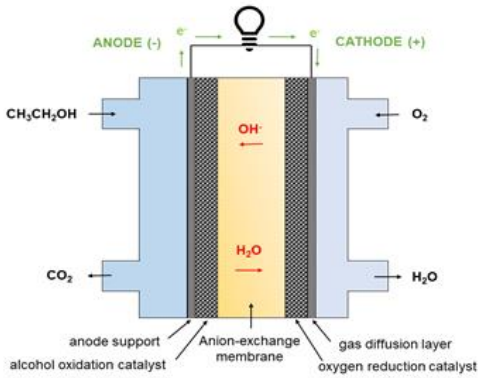

Fig. 1: Schematic illustration of an ADEFC (taken from Reference [1]).

EXPERIMENTAL

Both electrodes, the anode and the cathode were prepared by using an ultrasonic spraycoater to deposit the inks, consisting of catalyst, water, isopropanol, on the gas diffusion layers (GDLs). On the anode side a carbon cloth (ELAT - Hydrophilic Plain Cloth) and on the cathode side a carbon paper (Sigracet 29 BC) was utilized as GDL. The electrodes showed a metal loading of 0.75 mg cm^{-2} of the PdNiBi/C catalyst [2] for the ethanol oxidation reaction (EOR) and 0.5 mg cm^{-2} of the commercial PtRu/C catalysts for the oxygen reduction reaction.

For the investigation of the performance, a membrane electrode assembly (MEA) was prepared (Fig. 2) by putting the electrodes and the pretreated fumasep® membrane

(24h in 1 M KOH) together and afterwards assembled in the single cell. The single cell measurement was performed by using 1 M potassium hydroxide and 1 M ethanol as anode fuel and pure oxygen gas as cathode feed gas. [3] The cell potential (V) was recorded while increasing current densities (I) were applied at different temperatures (RT, 35°C, 43°C, 50°C, 57°C) to plot the I-V and I-P curves.

After the cell measurement the surface and morphology of the electrodes were characterized by using scanning electron microscopy (SEM).

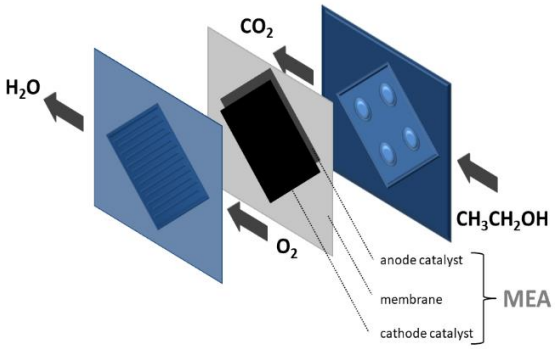

Fig. 2: Arrangement of the MEA between the flow fields (taken from Reference [1]).

RESULTS

The results of the single cell measurement are shown in Fig. 3. A maximum power density of 5 mW cm^{-2} was achieved.

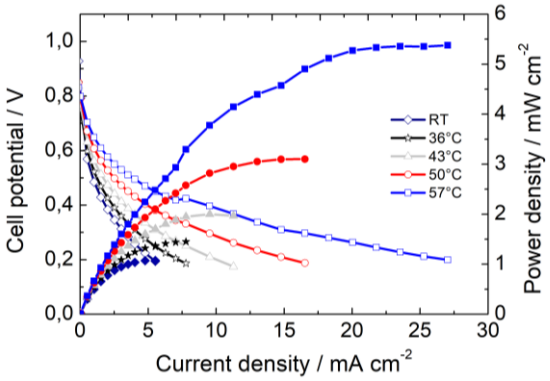

Fig. 3: Results of the single cell measurements.

The catalysts are well distributed on the carbon paper as well as on the carbon cloth. Only small agglomerates or some larger particles are visible. Further details are discussed in the poster presentation.

ACKNOWLEDGEMENT

The authors acknowledge the financial support by the Austrian Science Fund (FWF): I 3871-N37.

REFERENCES

[1] M. Roschger, S. Wolf, D. Garstenauer, V. Hacker, Proceedings of the 16th Minisymposium Verfahrenstechnik and 7th Partikelforum, 2020.

[2] B. Cermenek, B. Genorio, T. Winter, S. Wolf, J.G. Connell, M. Roschger, I. Letofsky-Papst, N. Kienzl, B. Bitschnau, V. Hacker, Electrocatalysis, 2020, 11, 203–214.

[3] A. M. Samsudin, S. Wolf, M. Roschger, V. Hacker, Int. Journal of Renewable Energy Development, 2021, 10(3), 435-443.

FUEL CELLS FOR FUTURE MOON MISSIONS

ROHDE Sebastian[1], HACKER Viktor[2], GOLLAS Bernhard[1] and COWLEY Aidan[3]

[1]Institute for Chemistry and Technology of Materials, Stremayrgasse 9, A-8010 Graz, Austria, sebastian.rohde@tugraz.at, bernhard.gollas@tugraz.at
[2]Institute of Chemical Engineering and Environmental Technology, Inffeldgasse 25/C, A-8010 Graz, viktor.hacker@tugraz.at
[3]European Astronaut Centre, Linder Höhe, D-51147 Cologne, Germany, aidan.cowley@esa.int

Keywords: fuel cell, ISRU, accelerated stress test, moon, catalyst poison, novel catalysts, MEA fabrication

Fuel cell (FC) and electrolyser (EC) systems are a vital and space proven technology supporting the upcoming expansion of human presence into the solar system. In particular, unitized regenerative FCs pose an elegant energy storage solution. They are a robust power system benefiting from the high energy density of hydrogen while they can also be operated in reverse to electrolyse water (potentially derived from In-situ resource utilization (ISRU) processes) creating fuel on demand. However, while these properties are very promising, this technology needs to be adapted in order to endure harmful constituents in ISRU derived resources. For example, in the case of lunar ISRU, according to a publication from Colaprete et al. [1] large amounts of H2S, NH3, SO2 and CH3OH were spectroscopically detected alongside water in an ejecta plume originating from an impact into a permanently shadowed crater. All these chemicals are well-known catalyst poisons causing a premature system degradation and failure. Notably H2S and SO2 are problematic since conventional FCs require essentially sulphur free feed gases with a sulphur compound limit of only a few ppb. On earth these impurities are removed using complex energy intensive purification-methods before the fuel is in a usable condition, yet in the extreme environment of a lunar outpost less costly solutions will be essential. Thus, this work aims to study and improve the FC/EC resistance against ISRU derived catalyst poisons by introducing said impurities into the feed gas accompanied with accelerated stress tests. This will be accomplished by fabricating robust membrane electrode assemblies with novel catalyst systems and state-of-the-art fabrication methods. The output from this study would give the exploration community a fundamental insight into the behaviour of ISRU process output interactions with FC/EC stack technology - a critical understanding in successfully developing robust energy systems for Lunar but also Martian exploration.

REFERENCES

[1] A. Colaprete, P. Schultz, J. Heldmann, D. Wooden, M. Shirley, K. Ennico, B. Hermalyn, W. Marshall, A. Ricco, R. C. Elphic, D. Goldstein, D. Summy, G. D. Bart, E. Asphaug, D. Korycansky, D. Landis and L. Sollitt, “Detection of Water in the LCROSS Ejecta Plume,” Science, vol. 330, p. 463–468, 2010.

DEVELOPMENT OF QPVA/PDDA ANION EXCHANGE MEMBRANES FOR ALKALINE FUEL CELLS

SAMSUDIN Asep Muhamad[1,2] and HACKER Viktor[1]

[1]Institute of Chemical Engineering and Environmental Technology, Graz University of Technology, Austria, asep.samsudin@tugraz.at
[2]Department of Chemical Engineering, Diponegoro University, Indonesia

Keywords: AEMs, Fuel Cells, QPVA, PDDA, Crosslinking.

INTRODUCTION

Anion exchange membranes (AEMs) have an essential role in enhancing the performance and efficiency of alkaline polymer electrolyte fuel cells. To achieve desirable performance, high ion-conductivity, excellent mechanical structure, and good stability are needed. Quaternized polymers were extensively used for anion-exchange membranes (AEMs) fabrication. Nevertheless, the complexity of the quaternization process and the use of toxic or carcinogenic components become the foremost issues in their development [1].

In this study, we prepared AEMs with quaternary ammonium poly(vinyl alcohol) (QPVA) as the main-backbone polymer and poly(diallyldimethylammonium chloride) (PDDA) as an ion-conducting source. Poly(vinyl alcohol) (PVA) is a polymer with excellent film-forming properties, hydrophilic, and non-toxic. A high density of reactive chemical functional groups in PVA structure is beneficial for crosslinking and chemical modification. Additionally, PVA has a low methanol permeability. PDDA can offer quaternary ammonium groups as OH^- conductors. Furthermore, the degradation of the quaternary ammonium through S_N2 nucleophilic substitution in alkaline environments can be hindered owing to the high steric hindrance due to the cyclic structures of PDDA. PDDA is also environment-friendly [2].

To restrain membrane swelling and improve the membrane's chemical stability, crosslinking of the polymer chains was introduced to the membrane preparation. The effect of the concentration of the chemical crosslinker for QPVA/PDDA AEMs was investigated.

EXPERIMENTAL

Membranes Preparation. Initially, 10 ml of 2 M KOH solution and 10 g GTMAC were added to the 5% PVA solution under continuous stirring for 4 h at 65°C. The resulting mixture was washed with anhydrous ethanol to obtain the precipitate and dried at 60°C for 24 h. Finally, the white QPVA particles were obtained. QPVA was dissolved in ultra-pure water at 80-90^{o}C while continuously stirring to acquire 10 wt.% QPVA. Then 10 wt.% PDDA was mixed with the QPVA in a weight ratio of 1:0.5 with continuous stirring for 4 h. The resulted solution was cast onto the glass surface with Elcometer 4340 automatic film applicator and evaporated under ambient conditions for 24h. Afterward, the membranes were peeled from the glass substrate.

Crosslinking. The membranes were annealed at 130 ^{o}C for an hour and soaked in different glutaraldehyde-based crosslinker solutions to induce crosslinking between PVA chains.

Characterization. Water uptake (WU), swelling degree in-plane (SD-i), and swelling degree through-plane (SD-t) were evaluated, measuring the change in weight and area and thickness of the membrane before and after hydration. The OH^- conductivity was measured by an AC impedance technique using electrochemical impedance spectroscopy.

RESULTS

Fig. 1 shows water uptake (WU), swelling degree in-plane (SD-i), and swelling degree through-plane (SD-t) of AEMs. We can see that WU increases with the rise of GA concentration. Resulting in maximum water uptake of 90% for GA 12.5 membranes. The increase of SD through-plane is proportional to the increase of WU. There are no significant changes in SD in-plane, which means that swelling is more likely to occur vertically. Fig. 2 shows the OH^- conductivity of membranes. Conductivity enhances with the increase of GA concentration. The increase of OH^- conductivity (σ) could be due to the increase in water content present in the membrane (water uptake). The membrane with GA 12.5 treatment acquired the highest hydroxide conductivity, water uptake, swelling degree, and mechanical strength.

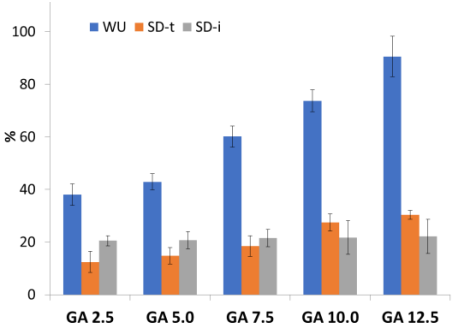

Fig. 1 WU, SD-t, and SD-i of AEMs

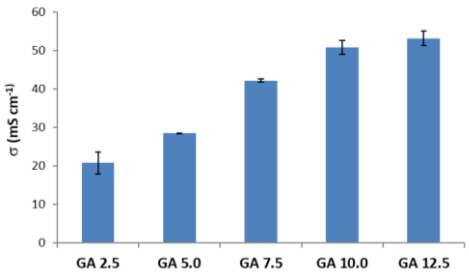

Fig. 1 OH^- Conductivity of AEMs

ACKNOWLEDGMENT

This work was supported by the Austrian Science Fund (FWF) project no. I 3871-N37 and the Indonesia-Austria Scholarship Programme (IASP).

REFERENCES

[1] A.M. Samsudin, S. Wolf, M. Roschger, and V. Hacker, International Journal of Renewable Energy Development, 10, (2021) p435-443

[2] A. M. Samsudin and V. Hacker, J. Electrochem. Soc., 168, (2021), p044526

THE EFFECT OF THE STRUCTURE OF CARBON SUPPORTS ON THE OXYGEN REDUCTION REACTION ACTIVITY OF SUPPORTED ZIRCONIA CATALYSTS IN AN ACIDIC ELECTROLYTE

SERIZAWA Kohei[1], NAGAI Takaaki[2], IKEGAMI Kaoru[2], MONDEN Ryuji[2], OHGI Yoshiro[3], MITSUSHIMA Shigenori[1,2], ISHIHARA Akimitsu[2] and KURODA Yoshiyuki[1,2]

[1]Grad. School of Eng. Sci., Yokohama Natl. Univ., Japan, cel@ynu.ac.jp
[2]Inst. of Adv. Sci., Yokohama Natl. Univ., Japan.
[3]Kumamoto Ind. Res. Inst., Japan.

Keywords: zirconia, oxygen reduction reaction, graphene, carbon nanotube, cluster catalyst

INTRODUCTION

Pt catalysts used in large quantities for polymer electrolyte fuel cells (PEFCs) have problems with stability and cost. The oxides of group 4/5 metals are expected as alternative oxygen reduction reaction (ORR) catalysts which are stable under acidic conditions; however, metal oxide catalysts are usually less conductive. Previous studies have shown that the deposition of ZrO_x nanoparticles on a carbon nanotube with amorphous carbon was effective to improve conduction path to the active sites [1], though the amorphous carbon is easily degraded. In this study, ZrO_x was deposited via sol-gel reaction without the formation of amorphous carbon, and the structure of carbon supports to improve surface area and conduction path was investigated.

EXPERIMENT

Table.1 shows the synthesis conditions of the samples.

Carbon supports were dispersed in toluene containing $Zr(OBu)_4$ (N-methylpyloridone was also dissolved when N-CNT was used), stirred at room temperature for 1-3 days. Furthermore, the obtained solids were heated at 1000 [°C] for 1 [h] under N_2, Ar, or 4 [%] H_2/Ar flow (100 [mL min^{-1}]) [2].

Table 1 Synthesis conditions of samples

Sample name	Carbon support
GO (Non-Reduced)	GO_Powder_refrigerator (Water) 0.1 [g]
GO (Ar Reduced)	GO_Powder_refrigerator (Water) 0.1 [g]
GO+N-CNT(Ar Reduced)	GO_Powder_Water coexisting room temperature 0.1 [g]+N doped MWCNT 10 [mg]
GO+N-CNT(N_2 Reduced)	GO_Powder_Water coexisting room temperature 0.1 [g]+N doped MWCNT 10 [mg]
GO+N-CNT(4 [%]H_2 Reduced)	GO_Powder_Water coexisting room temperature 0.1 [g]+N doped MWCNT 10 [mg]

The catalyst was dispersed in a mixture of 1-hexanol and 5 [wt %] Nafion® solution, and dried on a glassy carbon (GC) electrode. Electrochemical test was performed in a three-electrode cell without the rotation of the working electrode. The sample electrode, a GC plate, and the reversible hydrogen electrode (RHE) were used as working, counter, and reference electrodes, respectively, in a 0.5 [M] H_2SO_4 as an electrolyte. The pretreatment was performed by the 600 cycles of cyclic voltammetry (CV) between

0.05 and 1.20 [V vs. RHE] at 150 [mV s^{-1}] under N_2 atmosphere. The 3rd cycles of CV between 0.05 and 1.20 [V vs. RHE] at 50 [mV s^{-1}] was used for the estimation of the electric double layer capacitance. Those cycles at 5 [mV s^{-1}] under N_2 (i_{N2}) and O_2 (i_{O2}) atmospheres were measured and the ORR current density (i_{ORR}) was calculated from i_{N2}-i_{O2}.

The catalysts were characterized by X-ray diffraction (XRD), scanning electron microscopy (SEM), and N_2 adsorption measurement (BET).

RESULTS AND DISCUSSION

From XRD, tetragonal ZrO_2 was the major phase for the samples before reduction, though the peaks that could be attributed to monoclinic ZrO_x was also observed in the reduced sample. From SEM, In the reduced sample, ZrO_x nanoparticles were observed uniformly dispersed on the surface of the GO sheet. However, ZrO_x was agglomerated on N-CNTs in the samples containing both GO and N-CNT. In those samples, the lamination of the GO sheets was observed, and the N-CNT was dispersed among GO sheet. The orange bars in the Fig. 1 show the surface areas estimated by the BET method. The surface area was increased by the reduction treatment and/or the use of both GO and N-CNT. TG-DTA method indicated that support capacity of ZrO_x increases by reducing processing, while it decreases by compounding of carbon materials.

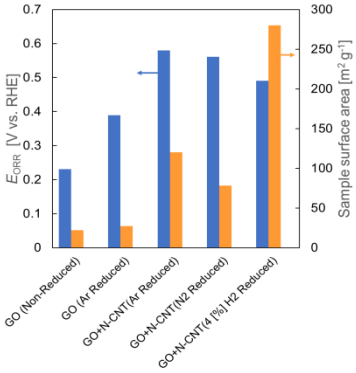

Fig. 1 Relationship between surface area and ORR starting potential of each sample

Fig. 2 shows the i_{ORR} normalized by the mass of ZrO_x. Here, the mass of ZrO_x was estimated from the residual mass of catalysts at 1000 [°C] by the TG-DTA. Fig. 1 shows the relationship between the surface area of each sample and the onset potential of ORR, E_{ORR} (potential of i_{ORR} ≤-1.0 [mA mg^{-1}]). Samples containing both GO and N-CNT have the onset potentials 0.19 [V vs.RHE] higher than those of the samples without N-CNT. The improved conductivity and surface area due to the addition of N-CNT probably originated the increase of the ORR activities.

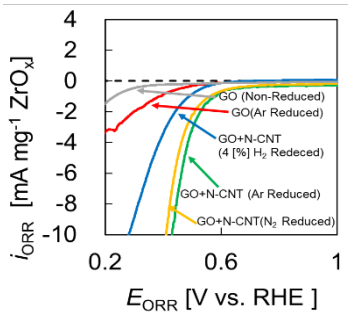

Fig. 2 Polarization curves of ZrO_x on various supports.

CONCLUSION

These results indicate that GO is useful as a support for high dispersion of ZrO_x nanoparticles, whereas it is necessary to improve conductivity and surface area by the addition of carbon materials such as N-CNTs.

REFERENCES

[1] A. Ishihara, T. Nagai, K. Ukita, M. Arao, M. Matsumoto, L. Yu, T. Nakamura, O. Sekizawa, Y. Takagi, K. Matsuzawa, T. W. Napporn, S. Mitsushima, T. Uruga, T. Yokoyama, Y. Iwasawa, H. Imai, and K. Ota, J. Phys. Chem. C, Vol. 123 (2019), pp.18150-18159.

[2] S. Takenaka, S. Miyake, S. Uwai, H. Matsune, and M. Kishida, J. Phys. Chem. C, Vol. 119 (2015), pp.12445-12454.

THE EFFECT OF CATHODE CATALYST LOADING FOR TOLUENE DIRECT ELECTRO-HYDROGENATION USING MEMBRANE ELECTROLYZER

SUGITA Yuya[1], NAGASAWA Kensaku[2], KURODA Yoshiyuki[1,2] and MITSUSHIMA Shigenori [1,2]

[1]Graduate School of Engineering Science, Yokohama National University, 79-5 Tokiwadai, Hodogaya-ku, Yokohama 240-8501, Japan.
[2]Institute of Advanced Sciences, Yokohama National University, 79-5 Tokiwadai, Hodogaya-ku, Yokohama 240-8501, Japan.
E-mail: cel@ml.ynu.ac.jp

Keywords: Organic chemical hydride, Membrane electrolysis, Catalyst layer, Catalyst loading

INTRODUCTION

Recently, renewable energy has been expected to reduce carbon dioxide emission. To utilize fluctuated and uneven distributed renewable energy effectively, large-scale hydrogen storage and transportation systems as the secondary energy have been required. Toluene (TL) / methylcyclohexane (MCH) organic chemical hydride system is an attractive candidate for hydrogen energy carrier to solve these requirements. This system is easy to handle because TL and MCH have low toxicity and exist in liquid state at the ambient temperature and pressure. Instead of conventional two-step of water electrolysis and chemical hydrogenation system, we have studied one-step direct electro-hydrogenation of toluene with water splitting using proton exchange membrane [1].

In this study, we investigated the effect of cathode catalyst loading for TL direct electro-hydrogenation to improve Faraday efficiency.

EXPERIMENTAL

The anode was ultra-fine mesh DSE® for oxygen evolution (De Nora Permelec, Ltd.), which was based on sintered titanium fiber plate. Carbon paper with micro porous layer (39BC; thickness=315 µm, SGL carbon ltd.) was used as the cathode flow field. On this carbon paper, 0.02 mg cm^{-2} of platinum catalyst was dispersed by the impregnation method for chemical hydrogenation using by-product of hydrogen. Electrocatalyst of cathode was Pt-Ru/C (Pt: 30 wt.%, Ru: 23 wt.%, TEC61E54, Tanaka Kikinzoku Kogyo). This electrocatalyst was mixed with ionomer (ionomer – carbon ratio was 0.8) using ball mill and coated on proton exchange membrane (Nafion 117®, Du Pont) using bar coater and masks. Then, we changed the cathode catalyst loading amount from 0.25 to 2.45 mg cm^{-2} by adjusting the thickness of the masks. The catalyst coated membrane was hot-pressed on the carbon paper at 120°C and 0.25 MPa for 3 min to fabricate a membrane cathode assembly. Geometrical electrode area was 11.6 cm^2.

During electrolysis, cathode reactant of 10% toluene diluted by methylcyclohexane, and anode reactant of 1mol dm^{-3} H_2SO_4 were circulated at 20 mL min^{-1} and 10 mL min^{-1} respectively. Operation temperature was 60°C. As electrochemical measurements,

linear sweep voltammetry (LSV), electrochemical impedance spectroscopy (EIS), chronoamperometry (CA) and Faraday efficiency measurement were conducted. Faraday efficiency was determined with the volume ratio of generated hydrogen gas and toluene-methylcyclohexane solution obtained at the outlet of cathode chamber by Faraday's law.

RESULTS AND DISCUSSIONS

Fig. 1 shows *iR* corrected the anode and the cathode polarization curves. The anode polarization curves were not affected by the amount of cathode catalyst loading. On the other hand, the cathode polarization curves significantly changed with catalyst loadings in low current density region. The cathode overpotentials of 0.25 and 2.45 mg cm^{-2} significantly showed the discontinuous increase at 50 and 80 mA cm^{-2} respectively.

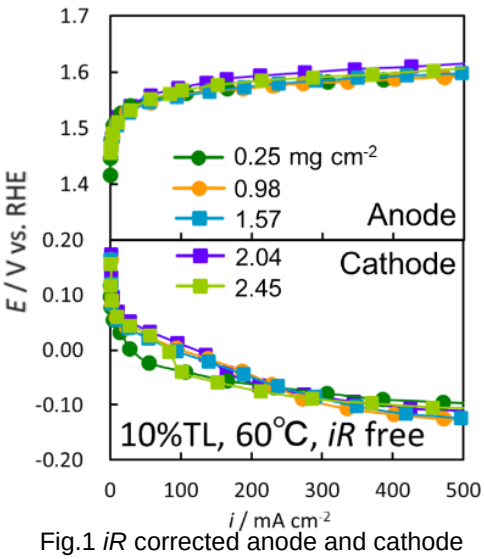

Fig.1 *iR* corrected anode and cathode polarization curves.

Fig. 2 shows Faraday efficiency as a function of current density. Higher Faraday efficiency was shown in the order of 1.57, 0.98, 2.04, 2.45 and 0.25 mg cm^{-2}. Then, the on-set current densities of Faraday efficiencies corresponded to discontinuous cathode overvoltage increases in Fig. 1. Therefore, the discontinuous increase of the cathode overpotentials were due to hydrogen evolution reaction. The reason for the decrease in Faraday efficiency under the too low or high loading of 0.25 or 2.45 might be as follows. If the loading is too low and the catalyst layer is too thin, most of the catalyst layer would be filled with MCH and drag water, which inhibit the supply of TL to the catalyst layer. In the case of too high loading and too thick catalyst layer, some catalyst layers, which is not used effectively, would prevent TL from moving to the reaction site.

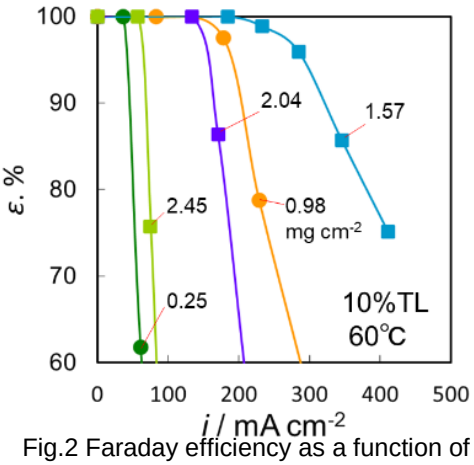

Fig.2 Faraday efficiency as a function of current density.

Fig. 3 shows the current density and the cathode potential at 90% of Faraday efficiency as a function of Pt-Ru loading. The current density increased with the catalyst loading up to 1.57 mg cm^{-2}. Above 1.57 mg cm^{-2}, the current density decreased with increasing catalyst loading. On the contrary, the cathode potential decreased with the increase of catalyst loading up to 1.57 mg cm^{-2}. After the cathode potential reached a minimum value at 1.57 mg cm^{-2}, it increased with catalyst loading. Thus, 1.57 mg cm^{-2} showed the highest Faraday efficiency even at the lowest the cathode potential. This result means that the selectivity of the cathode reaction should not be controlled by

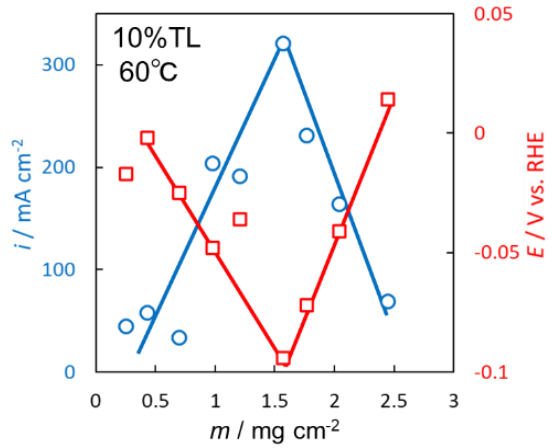

Fig.3 Current density (Circle) and cathode potential (Squire) at 90% of Faraday efficiency as a function of Pt-Ru loading.

kinetics of electrochemical reaction on the electrocatalyst, but strongly affected by mass transfer process of TL in the thickness direction of the catalyst layer.

ACKNOWLEGEMENTS

This work was based on results obtained from the Development of Fundamental Technology for Advancement of Water Electrolysis Hydrogen Production in Advancement of Hydrogen Technologies and Utilization Project (JPNP14021) commissioned by the New Energy and Industrial Technology Development Organization (NEDO). The anode was supplied by De Nora Permelec Ltd. We appreciate the person concerned them.

REFERENCE

[1] K. Nagasawa, K. Tanimoto, J. Koike, K. Ikegami, S. Mitsushima, J. Power Sources, 439, 227070 (2019).

HIGHLY ACTIVE SELF-REPAIRING ANODE CATALYST FOR ALKALINE WATER ELECTROLYSIS CONSISTING OF HYBRID NANOSHEET

TAKATSU Shohei[1], TANIGUCHI Tatsuya[2], OISHI Ayaka[2], NAGASHIMA Ikuo[2], INOMATA Akihiko[2], NISHIKI Yoshinori[3], AWALUDIN Zaenal[3], NAKAI Takaaki[3], KATO Akihiro[3], MITSUSHIMA Shigenori[1,4] and KURODA Yoshiyuki[1,4]

[1]Graduate school of Engineering Science, Yokohama National University, 79-5 Tokiwadai, Hodogaya-ku, Yokohama 240-8501, Japan.
[2]Kawasaki Heavy Industry, Ltd.,1-1 Kawasaki-cho, Akashi, Hyogo 673-8666, Japan.
[3]De Nora Permelec Ltd., 2023-15 Endo, Fujisawa, Kanagawa 252-0816, Japan.
[4]Institute of Advanced Sciences, Yokohama National University, 79-5 Tokiwadai, Hodogaya-ku, Yokohama 240-8501, Japan.
E-mail: cel@ml.ynu.ac.jp

Keywords: alkaline water electrolysis, Self-repairing catalyst, Oxygen evolution reaction, Nanosheet, Renewable energy

INTRODUCTION

Alkaline water electrolysis (AWE) is a promising system to convert renewable energy into chemical energy of hydrogen. However, electrodes likely degrade by frequent potential change and start/stop operation due to renewable energy.[1] We have previously reported that a hybrid cobalt nanosheet (Co-ns) is useful as a self-repairing catalyst under cycled potential, though further improvement of the oxygen evolution reaction (OER) activity is demanded.[2] Here, we report the activity and durability of synthesized hybrid nickel-iron hydroxide nanosheet (NiFe-ns) based on NiFe-layered double hydroxide, which is known as one of earth abundant catalysts with the highest activity for OER in alkaline medium.

EXPERIMENTAL

Aqueous solutions of 0.5 M tris(hydroxymethyl)aminomethane (Tris-NH_2) and 0.5 M metal chloride tetrahydrate (Ni/Fe = 9) were mixed together, and heated at 90°C for 2 days. The dispersion of NiFe-ns was separated by filtration using a membrane (pore size: 0.2 μm). The precipitate was washed with deionized water and separated twice. After drying at 90°C, an ocherous powder of the stacked NiFe-ns was obtained. The stacked NiFe-ns was redispersed in deionized water (10 mg mL^{-1}) by ultrasonication.

Electrochemical measurements were performed in a three-electrode cell with an Ni wire electrode etched in an HCl as a working electrode, a Ni coil as a counter electrode, and the RHE as a reference electrode (All potentials are hereafter denoted versus RHE.). The following deposition protocol was repeated until each OER overpotential becomes stable: i) constant current electrolysis (CP) at 800 mA cm^{-2} for 30 min, ii) a CV cycle at 0.5–1.8 V with the scan rate at 5 mV s^{-1}, iii) a CV cycle at 0.5–1.6 V with the scan rate at 50 mV s^{-1}, and iv) electrochemical impedance spectroscopy (EIS) under a constant current of 50 mA cm^{-2} at the frequency range 10^{-1}–10^{5} Hz. Current vibration with the amplitude 15 mA cm^{-2} was applied. The following test protocol was repeated for 20 times and a total number of potential cycles of 40,000. After 2,000 CV cycles at 0.5–1.8

V with the scan rate at 500 mV s^{-1} to apply the potential cycling stress, catalyst layer was repaired according to the protocol i) above and the catalytic activity was evaluated according to the protocols ii)–iv) above.

RESULTS AND DISCUSSION

The XRD pattern of NiFe-ns is shown in Fig.1. Although the peaks were broad, they can be attributed to the 001 (8.4º), 100 (34.3º), and 110 (60.7º) diffractions of pseudo hexagonal lattice. The lattice constants were *a* = 0.305 nm and *c* = 1.05 nm. These results are consistent with the formation of NiFe-ns as a hybrid metal hydroxide nanosheet similar to Co-ns.[2] In addition, ICP-AES showed that Ni/Fe = 1.45.

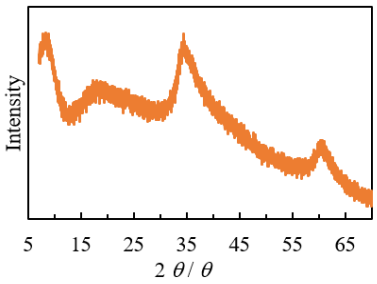

Fig. 1. XRD pattern of NiFe-ns powder.

Fig. 2 shows the changes of cyclic voltammograms during the catalyst deposition process. The redox peaks of Ni^{2+}/Ni^{3+} originating from NiFe-ns deposited on the electrode surface were observed at 1.38 V (anode) and 1.31 V (cathode). The OER overpotential at 100 mA cm^{-2} was 329 mV after 30 min of total CP time, whereas it was decreased to 308 mV after 240 min of total CP time, which indicates that NiFe-ns was deposited on the electrode by CP and act as a catalyst layer. The overpotential after the total CP time of 240 min was about 50 mV lower than that of Co-ns. Fig. 3 shows the change in OER overpotential for each 2000 cycles in the durability test. For bare Ni, the initial overpotential was 392 mV, and a significant increase in the overpotential with electrode corrosion was observed from around 8000 cycles, and finally increased to 485 mV. In contrast, Co-ns showed high durability, in which the overpotential changed from 350 mV to 359 mV after 40,000 cycles. The overpotential of NiFe-ns gradually decreased from 309 mV to 273 mV after about 20,000 cycles, and then remained stable until the 40,000th cycle (276 mV). The anodic Ni^{2+}/Ni^{3+} peak of NiFe-LDH in the cyclic voltammogram shifted to 1.43 V after 2000 cycles of the durability test, suggesting a structural change. After 2000 cycles, the peak current increased up to 3200 cycles, suggesting that the increase in the activity

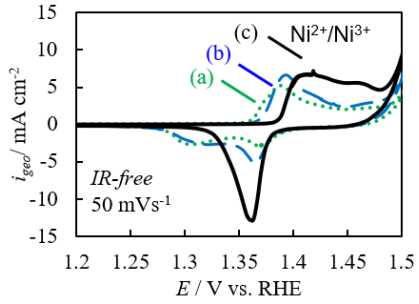

Fig. 2. CV curves of Ni wire coated with NiFe-ns during the catalyst deposition after (a) 30 min, (b) 60 min, and (c) 240 min of CP.

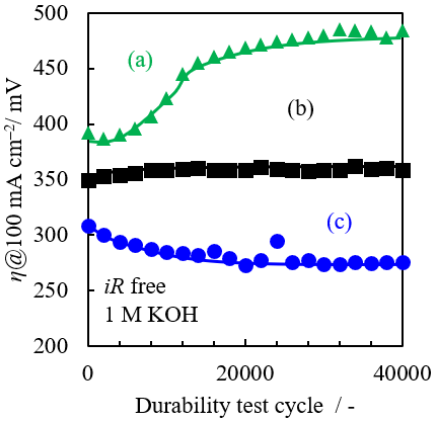

Fig. 3. OER overpotential (η) of (a) bare Ni, (b) Co-ns, and (c) NiFe-ns as a function of durability test cycle.

was correlated with the increase in the amount of deposited catalyst during the durability test. These results indicate that NiFe-ns, like Co-ns, has a high stability under fluctuating power supply and also has a higher OER activity than Co-ns.

In conclusions, we developed NiFe-ns dispersible in KOH and evaluated its performance of self-repairing catalyst. NiFe-ns showed high OER activity and high durability against fluctuating power supply.

REFERENCES

[1] Y. Uchino, T. Kobayashi, S. Hasegawa, I. Nagashima, Y. Sunada, A. Manabe,Y. Nishiki, S. Mitsushima, Electrocatalysis, 9, 64 (2018).
[2] Y. Kuroda, T. Nishimoto, S. Mitsushima, Electrochim. Acta, 323, 134812 (2019).

VISUALIZATION OF BUBBLE BEHAVIOR ON HYDROPHOBIC COATED CL IN PEM WATER ELECTROLYSIS CELL

WANI Koudai, ARAKI Takuto, NAGASAWA Kensaku and MITSUSHIMA Shigenori

Yokohama National University,Tokiwadai 79-5, Hodogaya-ku, Yokohama, 240-8501, Japan, wani-koudai-sk@ynu.jp, araki-takuto-tm@ynu.ac.jp, nagasawa-kensaku-st@ynu.ac.jp, mitsushima-shigenori-hp@ynu.ac.jp

Keywords: PEM electrolysis, oxygen bubble, visualization, hydrophobic

Due to the need for a new energy infrastructure, water electrolysis technology is receiving increased attention. [1,2] One of the serious problems is management of generated oxygen bubbles which inhibits water supply to the CL. Therefore, bubble behavior was observed on three types of CL with hydrophilic and hydrophobic surface by using a high-speed camera.

A single cell, shown in Fig. 1, was used for observing oxygen bubble behavior. Naffion-117 was used as PEM, and IrOx and Pt/C was used anode and cathode catalyst, respectively. Sinterd Ti with Pt plating was used for anode porous transport layer (PTL). Three types of PTFE coated CL were prepared: (a)no coating, (b)coated half and (c)coated all. High-speed camera (Redlake MASD, HS-1), magnifying glass (Hirox, cx-10c) and objective lens (Hirox, OL-35) were used. Electrochemical measurement system (Bio-Logic, SP-240) was used for applying current, and the current density was unified at 477 mA / cm^2 so that the amount of generated oxygen was equal.

A big one bubble covering entire PTL hole was visualized in Fig. 2 (c). In Fig. 2(b), smaller bubbles appeared from left PTFE uncoated area were merged into a bigger bubble, which stayed on right PTFE coated area. The bubble size in Fig. 2 (a) was smaller than those of (b, c) and the shape is more spherical.

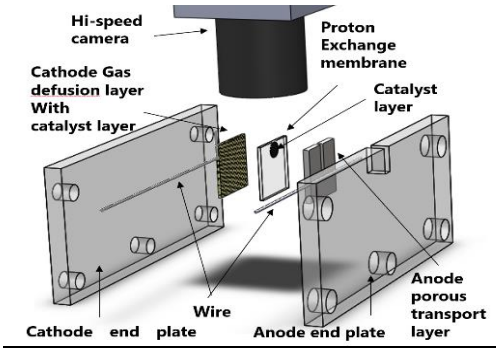

Fig.1 Achematic diagram

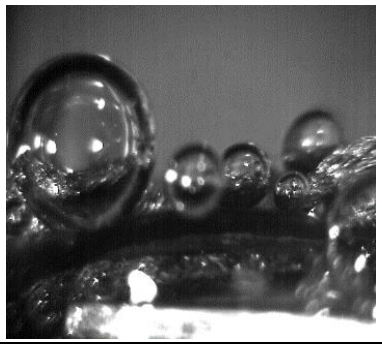

Fig.2(a) Not treated

Fig.2(b) Coated half

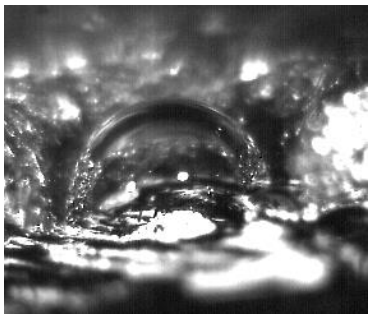

Fig.2(c) Coated all

ACKNOWLEDGEMENTS

This study was based on results obtained from a project (JPNP14021) commissioned by the New Energy and Industrial Technology Development Organization (NEDO).

REFERENCES

[1] G. Bender, M. Carmo et al, “Initial approaches in benchmarking and round robin testing for proton exchange membrane water electrolyzers”

[2] S. Mitsushima et al, ECS Meeting Abstracts, MA2019-02(2019), 1715.

ETHANOL TOLERANT CATALYSTS FOR THE OXYGEN REDUCTION REACTION IN ALKALINE DIRECT ETHANOL FUEL CELLS

WOLF Sigrid, ROSCHGER Michaela, GARSTENAUER Daniel and HACKER Viktor

TU Graz, Institute of Chemical Engineering and Environmental Technology, Inffeldgasse 25/C, 8010 Graz, Austria, sigrid.wolf@tugraz.at, viktor.hacker@tugraz.at

Keywords: Direct ethanol fuel cell, oxygen reduction reaction, cathode catalysts, rotating disk electrode analysis.

INTRODUCTION

In recent years, the increase in greenhouse gases and the resulting global warming due to the use of fossil fuels has become critical. Alkaline direct ethanol fuel cells (ADEFCs) are a promising technology for clean energy supply in mobile and stationary applications. Compared to equivalent technologies, ADEFCs promise advantages in terms of high performance, low toxicity and environmental friendliness and robustness. Ethanol, in addition to its relatively high energy density, is a comparatively easy-to-handle liquid and can be obtained on a large scale from agriculture and biomass. However, in addition to the incomplete oxidation of the fuel at the anode, the commercialization of ADEFCs is hindered by the ethanol crossover from the anode to the cathode, which leads to mixed potentials and fuel losses, reducing the fuel cell performance. Moreover, the cathode still suffers from heavy reliance on noble metal materials [1, 2]. To overcome these problems, the development of highly efficient, ethanol-tolerant cathode catalyst alternatives to replace the state-of-the-art platinum-based catalysts is one of the most important improvements needed. Oxygen reduction reaction (ORR) in alkaline media can occur according to two different pathways, the direct four-electron reduction (equation 1) and the less efficient, indirect two-step process forming hydrogen peroxide (equation 2) which is further converted to hydroxide ions (equation 3) [3].

$$O_2 + 2H_2O + 4e^- \rightarrow 4OH^- \qquad E° = 0.404\ V\ vs.\ RHE \qquad (1)$$

$$O_2 + H_2O + 2e^- \rightarrow HO_2^- + OH^- \qquad E° = 0.080\ V\ vs.\ RHE \qquad (2)$$

$$HO_2^- + H_2O + 2e^- \rightarrow 3OH^- \qquad E° = 0.880\ V\ vs.\ RHE \qquad (3)$$

EXPERIMENTAL

In this study, carbon supported cathode catalysts were prepared using a simple solvothermal synthesis method (Fig. 1). The synthesized catalysts were characterized ex-situ by means of thin-film rotating disk electrode experiments in a typical three electrode setup. In order to determine the oxidation and reduction processes and the activity towards oxygen reduction reaction, cyclic voltammograms and linear sweep voltammograms were recorded in N_2 purged 1 M potassium hydroxide solution. To gain information about the ethanol tolerance, the measurements are repeated in an alkaline ethanol solution (1 M). The number of transferred electrons is determined according to

Koutecky-Levich analysis. Chronoamperometry was performed to examine the stability of the catalysts.

RESULTS

The prepared catalysts show a high activity and stability towards ORR in the alkaline medium. Limiting current density values up to 16 mA/mg (Fig. 2) and transferred electron numbers examined with Koutecky-Levich of 3.4 could be achieved. In addition, a high tolerance to ethanol was determined.

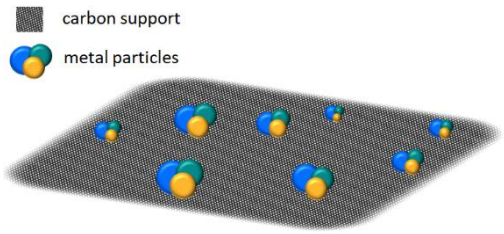

Fig. 1: Schematic illustration of metal particles on the carbon support forming the electrocatalysts.

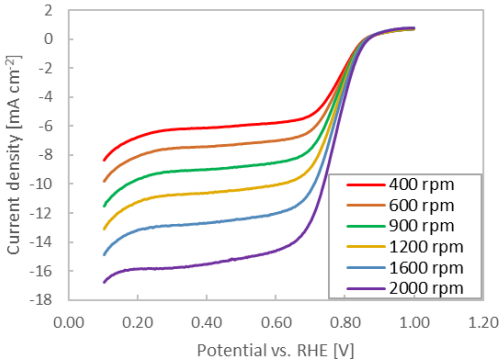

Fig. 2: Linear sweep voltammograms of synthesized cathode catalysts at 400-2000 rpm.

ACKNOWLEDGEMENT

The authors acknowledge the financial support by the Austrian Science Fund (FWF): I 3871-N37.

REFERENCES

[1] B. Cermenek, B. Genorio, T. Winter, S. Wolf, J.G. Connell, M. Roschger, I. Letofsky-Papst, N. Kienzl, B. Bitschnau, V. Hacker, Electrocatalysis, 2020, 11, 203–214.

[2] S. Wolf, M. Roschger, V. Hacker, Proceedings of the 16th Minisymposium Verfahrenstechnik and 7th Partikelforum, 2020.

[3] I. Grimmer, P. Zorn, S. Weinberger, C. Grimmer, B. Pichler, B. Cermenek, F. Gebetsroiter, A. Schenk, F.-A. Mautner, B. Bitschnau, V. Hacker, Elechtrochimica Acta, 2017, 228, 325-331.

Student Poster Presentation on
Hydrogen and Fuel Cells

within the 13th International Summer School on Advanced Studies of Polymer Electrolyte Fuel Cells

September 7th 2021

Institute of Chemical Engineering
and Environmental Technology, NAWI Graz
Graz University of Technology,
Inffeldgasse 25c, 8010 Graz, Austria

https://www.tugraz.at/institute/ceet/home/

Financial support was provided by the Austrian Ministry Climate Action, Environment, Energy, Mobility, Innovation and Technology, the Austrian Research Promotion Agency (FFG), the IEA Research Cooperation and TU Austria, the umbrella association of the Austrian Universities of Technology.